



# 1 Impact of reactive surfaces on the abiotic reaction between nitrite and 2 ferrous iron and associated nitrogen and oxygen isotope dynamics

3 Anna-Neva Visser<sup>1,4</sup>, Scott D. Wankel<sup>2</sup>, Pascal A. Niklaus<sup>3</sup>, James M. Byrne<sup>4</sup>, Andreas A. Kappler<sup>4</sup>,  
4 Moritz F. Lehmann<sup>1</sup>

5 <sup>1</sup>Department of Environmental Sciences, Basel University, Bernoullistrasse 30, 4056 Basel, Switzerland

6 <sup>2</sup>Woods Hole Oceanographic Institution, Woods Hole, 360 Woods Hole Rd, MA 02543, USA

7 <sup>3</sup>Department of Evolutionary Biology and Environmental Studies, University of Zürich, Winterthurerstrasse 190, 8057 Zürich,  
8 Switzerland

9 <sup>4</sup>Department of Geosciences, Tübingen University, Hölderlinstrasse 12, 72074 Tübingen, Germany

10 Correspondence to: Anna-Neva Visser (a.visser@unibas.ch)

11 **Abstract.** Anaerobic nitrate-dependent Fe(II) oxidation (NDFeO) is widespread in various aquatic environments, and plays a  
12 major role in iron and nitrogen redox dynamics. However, evidence for truly enzymatic, autotrophic NDFeO remains limited,  
13 with alternative explanations involving coupling of heterotrophic denitrification with abiotic oxidation of structurally-bound  
14 or aqueous Fe(II) by reactive intermediate N species (chemodenitrification). The extent to which chemodenitrification is  
15 caused, or enhanced, by *ex vivo* surface catalytic effects has, so far, not been directly tested. To determine whether the presence  
16 of either a Fe(II)-bearing mineral or dead biomass (DB) catalyses chemodenitrification, two different sets of anoxic batch  
17 experiment were conducted: 2 mM Fe(II) was added to a low-phosphate medium, resulting in the precipitation of vivianite  
18 ( $\text{Fe}_3(\text{PO}_4)_2$ ), to which later 2 mM nitrite ( $\text{NO}_2^-$ ) was added, with or without an autoclaved cell suspension ( $\sim 1.96 \times 10^8$  cells ml<sup>-1</sup>)  
19 of *Shewanella oneidensis* MR-1. Concentrations of nitrite, nitrous oxide ( $\text{N}_2\text{O}$ ) and iron ( $\text{Fe}^{2+}$ ,  $\text{Fe}_{\text{tot}}$ ) were monitored over  
20 time in both setups to assess the impact of Fe(II) minerals and/or DB as catalysts of chemodenitrification. In addition, the  
21 natural-abundance isotope ratios of  $\text{NO}_2^-$  and  $\text{N}_2\text{O}$  ( $\delta^{15}\text{N}$  and  $\delta^{18}\text{O}$ ) were analysed to constrain associated isotope effects. Up  
22 to 90% of the Fe(II) was oxidized in the presence of DB, while only ~65% were oxidized under mineral-only conditions,  
23 suggesting an overall lower reactivity of the mineral-only setup. Similarly, the average  $\text{NO}_2^-$  reduction rate in the mineral-only  
24 experiments ( $0.004 \pm 0.003$  mmol L<sup>-1</sup> day<sup>-1</sup>) was much lower compared to experiments with mineral plus DB ( $0.053 \pm 0.013$   
25 mmol L<sup>-1</sup> day<sup>-1</sup>), as was  $\text{N}_2\text{O}$  production ( $204.02 \pm 60.29$  nmol/L\*day). The  $\text{N}_2\text{O}$  yield per mole  $\text{NO}_2^-$  reduced was higher in the  
26 mineral-only setups (4%) compared to the experiments with DB (1%), suggesting the catalysis-dependent differential  
27 formation of NO. N- $\text{NO}_2^-$  isotope ratio measurements indicated a clear difference between both experimental conditions: in  
28 contrast to the marked <sup>15</sup>N isotope enrichment during active  $\text{NO}_2^-$  reduction ( $^{15}\epsilon_{\text{NO}_2} = +10.3\text{‰}$ ) observed in the presence of  
29 DB,  $\text{NO}_2^-$  loss in the mineral-only experiments exhibited only a small N isotope effect ( $< +1\text{‰}$ ). The nitrite O isotope effect  
30 was very low in both setups ( $^{18}\epsilon_{\text{NO}_2} < 1\text{‰}$ ), most likely due to substantial O isotope exchange with ambient water. Moreover,  
31 during the low-turnover conditions (i.e., in the mineral-only experiments, as well as initially in experiments with DB), the  
32 observed nitrite isotope systematics suggest, transiently, a small inverse isotope effect (i.e., decreasing nitrite  $\delta^{15}\text{N}$  and  $\delta^{18}\text{O}$ )



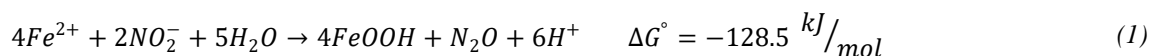
33 with decreasing concentrations), possibly related to transitory surface complexation mechanisms. Site preference (SP) of the  
34  $^{15}\text{N}$  isotopes in the linear  $\text{N}_2\text{O}$  molecule for both setups ranged between 1 to 7‰, notably lower than previously reported for  
35 chemodenitrification. Our results imply that chemodenitrification is dependent on the available reactive surfaces, and that the  
36  $\text{NO}_2^-$  (rather than the  $\text{N}_2\text{O}$ ) isotope signatures may be useful for distinguishing between chemodenitrification catalysed by  
37 minerals, chemodenitrification catalysed by dead microbial biomass, and possibly true enzymatic NDFeO.

## 38 1. Introduction

39 Iron (Fe) is essential for all living beings and its biogeochemical cycling has been studied extensively (Expert, 2012; Lovley,  
40 1997). Although Fe is ubiquitous in most environments, it is not always bioavailable (Andrews et al., 2003; Ilbert and  
41 Bonnefoy, 2013), and microorganisms must often cope with Fe limitation in their respective environments (Braun and Hantke,  
42 2013; Ilbert and Bonnefoy, 2013). This is especially true at circumneutral pH and oxic conditions, where Fe(II) is quickly  
43 oxidized by  $\text{O}_2$  and thus only present as poorly soluble Fe(III)(oxyhydr)oxides (Cornell and Schwertmann, 2003; Stumm and  
44 Sulzberger, 1992). In contrast, under anoxic conditions, Fe is mainly present as either dissolved  $\text{Fe}^{2+}$  or as mineral-bound Fe(II)  
45 in iron phosphates or carbonates (Charlet et al., 1990; Luna-Zaragoza et al., 2009). Here, microbes use electron acceptors other  
46 than  $\text{O}_2$  for respiration (He et al., 2016; Lovley, 2012; Straub et al., 1996). One redox pair that has been proposed to be exploited  
47 by microbes under anoxic conditions is  $\text{NO}_3^-/\text{Fe}^{2+}$ , through a mechanism known as nitrate-dependent Fe(II) oxidation (NDFeO)  
48 (Ilbert and Bonnefoy, 2013; Straub et al., 1996). Over the past two decades, several microorganisms have been investigated  
49 and reported to be either chemolithoautotrophic or -mixotrophic nitrate-dependent Fe(II)-oxidising bacteria (e.g. *Acidovorax*  
50 *delafieldii* strain 2AN, *Pseudogulbenkiania ferrooxidans* strain 2002) (Chakraborty et al., 2011; Weber et al., 2009). It has  
51 been suggested that extracellular electron transfer (EET) might play a major role in NDFeO (Liu et al., 2018). Particularly in  
52 the presence of high levels of extracellular polymeric substances (EPS) (Klueglein et al., 2014; Zeitvogel et al., 2017), which  
53 can act as electron shuttles, EET may indeed provide a plausible explanation for the observed Fe(II) oxidation in these cultures  
54 (Liu et al., 2018). The existence of such an electron transfer would imply that NDFeO is not necessarily a completely  
55 biologically catalysed reaction. Indeed, to date, genetic evidence that supports this metabolic capacity of the studied  
56 microorganisms remains lacking (Price et al., 2018), and biogeochemical evidence is rare and putative. The latter is mostly  
57 based on experiments with the chemolithoautotrophic culture KS, a consortium of four different strains, including a relative  
58 of the microaerophilic *Sideroxydans/Gallionella*. This enrichment culture has been shown to be able to oxidize Fe(II) without  
59 the addition of any organic co-substrates (Tominski et al., 2018). Tian et al. (2020) confirmed that *Gallionellaceae* are able to  
60 perform autotrophic Fe(II)-dependent denitrification. Another more indirect line of evidence includes results from slurry  
61 microcosm experiments with marine coastal sediments. In these experiments, Fe(II) oxidation was still detected even after all  
62 organics of the sediments were consumed and only nitrate was left (Laufer et al., 2016). With regards to other studies where  
63 NDFeO was initially thought to be performed by autotrophs (Chakraborty et al., 2011; Weber et al., 2009), it was subsequently  
64 shown that the microbes rely on an organic co-substrate and must in fact be considered mixotrophic (Klueglein et al., 2014;



65 Muehe et al., 2009). Yet, the exact mechanism promoting NDFeO is still not fully understood. Considering that all putative  
66 NDFeO strains were grown under high (up to 10 mM) nitrate ( $\text{NO}_3^-$ ) and Fe(II) concentrations, and accumulated up to several  
67 mM nitrite ( $\text{NO}_2^-$ ) from enzymatic  $\text{NO}_3^-$  reduction, it was suggested that the observed Fe(II) oxidation in these pure cultures  
68 may be due to the abiotic side reaction between the generated  $\text{NO}_2^-$  and Fe(II) (Buchwald et al., 2016; Prakash Dhakal, 2013;  
69 Klueglein et al., 2014). This abiotic reaction between  $\text{NO}_2^-$  and Fe(II) is known as chemodenitrification (Equation 1) and is  
70 proposed to lead to an enhanced production of  $\text{N}_2\text{O}$  (Anderson and Levine, 1986; Buchwald et al., 2016; Jones et al., 2015).



71 Several studies have noted that the presence of reactive surfaces may enhance the abiotic reaction (Heil et al., 2016; Sorensen  
72 and Thorling, 1991). For example, Klueglein and Kappler (2013) tested the impact of goethite on Fe-coupled  
73 chemodenitrification in the presence of high Fe(II) and  $\text{NO}_2^-$  concentrations, and confirmed the concentration dependency of  
74 this reaction with regard to both species (Van Cleemput and Samater, 1995). Possible catalytic effects (e.g. by reactive surfaces  
75 and/or organic matter) were not tested specifically in these studies. Yet, multiple factors have been shown to affect the abiotic  
76 reaction between  $\text{NO}_2^-$  and Fe(II) and may need to be considered (i.e.. pH, temperature,  $\text{Fe}^{2+}$  concentrations, solubility of  
77 Fe(III)(oxyhydr)oxides, crystallinity of Fe(II) minerals, other metal ion concentrations and catalytic effects) (Van Cleemput  
78 & Samater, 1995; Klueglein & Kappler, 2013; Ottley et al., 1997). In addition, the presence of organic compounds can lead to  
79 the abiotic reduction of  $\text{NO}_2^-$  to NO (Van Cleemput and Samater, 1995; McKnight et al., 1997; Pereira et al., 2013).

80 Given the complex controls and potential interaction between Fe(II) and various nitrogenous compounds, including  
81 intermediates, it may be an oversimplification to state that Fe(II) oxidation observed in previous laboratory setups is solely  
82 caused by the abiotic reaction with  $\text{NO}_2^-$ , and not, for example, stimulated by reactive surfaces (minerals, organic-detritus) or  
83 by nitric oxide (NO), a highly reactive intermediate not easily quantified in anoxic experiments. In order to better understand  
84 the factors that may control chemodenitrification of  $\text{NO}_2^-$ , this study focuses on the possible catalytic surface effects induced  
85 by a Fe(II) mineral phase or DB. Furthermore, microbial cells, dead biomass, or detrital waste products might not only provide  
86 additional reactive surface area, but may directly react with  $\text{NO}_2^-$  to form NO.

87 Stable isotopes of both N and O ( $\delta^{15}\text{N}$  and  $\delta^{18}\text{O}$ ) offer a promising approach to further elucidate the mechanism of NDFeO,  
88 and also to more generally expand our understanding of chemodenitrification. The N and O isotopic composition of  
89 nitrogenous compounds (e.g.,  $\text{NO}_3^-$ ,  $\text{NO}_2^-$ , and  $\text{N}_2\text{O}$ ) has been used to gain deeper insights into various N turnover processes  
90 (Granger et al., 2008; Jones et al., 2015). The dual  $\text{NO}_2^-$  (or  $\text{NO}_3^-$ ) isotope approach is based on the fact that specific N-  
91 transformation processes – biotic or abiotic – are associated with specific N and O isotope fractionation (i.e., isotope effect).  
92 In general, enzymatic processes promote the more rapid reaction of lighter N and O isotopologues, leaving the remaining  
93 substrate pool enriched in the heavier isotopes (i.e.,  $^{15}\text{N}$ ,  $^{18}\text{O}$ ) (Granger et al., 2008; Kendall & Aravena, 2000; Martin &  
94 Casciotti, 2017). Only a few studies exist that have looked into the isotope effects of chemodenitrification and reports on the  
95 associated isotope effects are variable. Consistent with what we know from biological denitrification, chemodenitrification  
96 experiments with 10 mM Fe(II) and  $\text{NO}_2^-$ , with very high reaction rates, revealed a significant increase in the  $\delta^{15}\text{N}$  (up to 40%)



97 and  $\delta^{18}\text{O}$  (up to 30‰)  $\text{NO}_2^-$  values, corresponding to an overall N and O isotope effect of  $^{15}\epsilon$   $18.1 \pm 1.7\%$  and  $^{18}\epsilon$   $9.8 \pm 1.8\%$ ,  
98 as well as a  $\Delta^{15}\text{N}$  (i.e., the difference between  $\delta^{15}\text{NO}_2^-$  and  $\delta^{15}\text{N}_2\text{O}$ ) of  $27 \pm 4.5\%$  (Jones et al., 2015). This suggests that  
99 coupled N and O isotope measurements hold the potential to disentangle abiotic and biotic  $\text{NO}_2^-$  reduction in the presence of  
100 Fe(II). Here, in order to expand the limited dataset on the isotope effects of abiotic Fe(II)-coupled denitrification, and in turn  
101 to lay the groundwork for using  $\text{NO}_3^-/\text{NO}_2^-$  N and O isotope measurements to unravel the mechanism behind NDFeO, we  
102 studied the N and O isotope dynamics of  $\text{NO}_2^-$  reduction and  $\text{N}_2\text{O}$  production during abiotic reaction of  $\text{NO}_2^-$  with Fe(II). As  
103 the extent of the formation of various Fe(III)(oxyhydr)oxides has been previously reported to enhance chemodenitrification  
104 dynamics (Chen et al., 2018; Sorensen and Thorling, 1991), we also followed mineral alteration during chemodenitrification  
105 in order to identify possible reaction patterns. A specific goal in this context was to assess the impact of Fe(II) precipitates  
106 and/or dead biomass as catalytic agents during Fe(II)-associated chemodenitrification, as well as potential mineral  
107 transformation processes associated with the abiotic oxidation of Fe(II) via reactive  $\text{NO}_x$  species.

## 108 2. Material and Methods

### 109 2.1. General experimental setup

110 For all experiments, anoxic low phosphate medium (1.03 mM  $\text{KH}_2\text{PO}_4$ , 3.42 mM NaCl, 5.61 mM  $\text{NH}_4\text{Cl}$ , 2.03 mM  $\text{MgSO}_4 \cdot 7$   
111  $\text{H}_2\text{O}$  and 0.68 mM  $\text{CaCl}_2 \cdot 2 \text{H}_2\text{O}$ , with a 7-vitamin (Widdel & Pfennig, 1981) and a SL-10 trace element solution (Widdel et  
112 al., 1983); 22 mM bicarbonate buffered) was prepared. The medium was dispensed with a Widdel flask in 1-l Schott bottles  
113 and the pH for each bottle was adjusted separately by the addition of anoxic, sterile 1 M HCl. For the both setups, five different  
114 pH values were targeted: 5.8, 6.2, 6.5, 6.9 and 7.1. After pH adjustment, Fe(II)Cl<sub>2</sub> was added to reach a concentration of ~2  
115 mM Fe(II), and, if necessary, the pH was re-adjusted. The medium was kept for 48 h at 4°C, resulting in amorphous, green-  
116 greyish Fe(II) precipitates. In addition, ~2 mM  $\text{NaNO}_2$  and ~1 mM Na-acetate were added to the main medium stocks shortly  
117 before 10 ml aliquots of the medium were distributed into 20 ml headspace vials (heat-sterilized) in an anoxic glove box  
118 (MBraun,  $\text{N}_2$ , 100%). Acetate was added to mimic experiments, in which bacteria are cultivated (yet, acetate concentrations  
119 did not change during incubations, underscoring that the organic acid was not involved in the observed reactions; data not  
120 shown). All headspace vials were closed with black butyl stoppers and crimp-sealed [headspace  $\text{N}_2/\text{CO}_2$  (90/10, v/v)]. All vials  
121 were then incubated at 28°C in the dark.

122 *Incubations with dead-biomass* – *Shewanella oneidensis* MR-1, a facultatively aerobic Gram-negative bacterium, is seen as  
123 model organism for bioremediation studies due to its various respiratory abilities (Heidelberg et al., 2002; Lies et al., 2005). It  
124 is known to perform dissimilatory metal reduction by utilizing alternative terminal electron acceptors such as elemental sulfur,  
125 Mn(IV), Fe(III) or  $\text{NO}_3^-$ . Since *S. oneidensis* produces large amounts of EPS (Dai et al., 2016; Heidelberg et al., 2002), but is  
126 not capable of oxidizing Fe(II) (Lies et al., 2005; Piepenbrock et al., 2011) (i.e. no interference with abiotic reactions involving  
127 Fe/chemodenitrification), we chose concentrated and sterilized *S. oneidensis* for our dead-biomass experiments. In preparation  
128 of these experiments, *S. oneidensis* MR-1 was grown oxically on a LB (lysogeny broth) medium (10 g tryptone, 5 g yeast



129 extract, 10 g NaCl in 1 l DI water) in six 250 ml Erlenmeyer flasks. After 12 hrs, cultures were transferred into 50 ml Falcon  
130 tubes and centrifuged for 25 min at 4000 rpm (Eppendorf, 5430 R). Cell-containing pellets were washed twice with oxalic acid  
131 and centrifuged again, followed by three more washing steps with TRIS buffer prior to final resuspension in 5 ml TRIS buffer.  
132 Pellet suspensions were pooled in a 100 ml serum bottle and autoclaved twice to ensure that all cells were killed. Before  
133 distribution of the medium into 20 ml vials (see above), cell suspension was added to yield a cell density of  $\sim 1.96 \times 10^8$  cell ml<sup>-1</sup>.  
134 Care was taken to ensure the homogenous distribution of mineral precipitates and the dead biomass.

## 135 2.2. Sampling and sample preparation

136 Incubations were run for approximately 30 days, and sampling was performed in an anoxic glove box (MBraun, N<sub>2</sub>, 100%) at  
137 five time points. For each time point, and for each pH treatment, 9 replicates were prepared. Therefore, variations between the  
138 replicates and the different sampling time points are possible. For sampling, the headspace was quantitatively transferred into  
139 12 ml He-purged Exetainer vials (LABCO) for N<sub>2</sub>O concentration measurements. Then, 2 ml of the liquid sample were  
140 transferred into 2 ml Eppendorf tubes, centrifuged 5 min (13400 rpm; Eppendorf, MiniSpin), followed by a 1:10 dilution of  
141 the supernatant in 1 ml anoxic MilliQ water for NO<sub>2</sub><sup>-</sup> quantification. A second 100 µl aliquot was diluted 1:10 in 40 mM  
142 sulfamic acid (SFA) for iron determination by ferrozine analysis (Granger and Sigman, 2009; Klueglein and Kappler, 2013).  
143 The remaining supernatant was used for HPLC and NO<sub>2</sub><sup>-</sup> isotope analysis. Finally, the spun-down pellet was resuspended in 1  
144 M HCl for ferrozine analysis (Stookey, 1970). All samples were stored at 4°C in the dark until further processing. The  
145 remaining liquid samples were used for <sup>57</sup>Fe Mössbauer spectroscopy.

## 146 2.3. Analytical techniques

147 *NO<sub>2</sub><sup>-</sup> concentrations* – NO<sub>2</sub><sup>-</sup> concentrations were quantified using standard segmented continuous-flow analytical (CFA, SEAL  
148 Analytics) photometric techniques (Snyder and Adler, 1976). NO<sub>2</sub><sup>-</sup> reduction rates were calculated based on the observed net  
149 concentration decrease ( $\overline{[C]}_{t_0} - \overline{[C]}_{t_{end}} \pm \text{standard error}$ ) with time.

150 *Fe concentrations* – Fe(II) concentration was analysed using the ferrozine assay (Stookey, 1970), which was adapted for NO<sub>2</sub><sup>-</sup>  
151 -containing samples by Klueglein et al. (2013). Total Fe(II) concentrations were calculated as the sum of the  $Fe_{aq}^{2+} +$   
152  $Fe(II)_{pellet}$  concentrations.

153 *N<sub>2</sub>O concentrations* – Prior to the quantification of the N<sub>2</sub>O, the sample gas was diluted (1:5) with 5.0 He. The samples were  
154 then analysed using a gas chromatograph with an electron capture detector (GC-ECD; Agilent 7890 with micro-ECD and FID;  
155 Porapak Q 80/100 column). GC-ECD measurements were calibrated using four standard gases containing different  
156 concentrations of N<sub>2</sub>O (Niklaus et al., 2016). N<sub>2</sub>O production rates were calculated based on the observed net N<sub>2</sub>O  
157 concentration increase ( $\overline{[C]}_{t_{end}} - \overline{[C]}_{t_0} \pm \text{standard error}$ ) with time.

158 *<sup>57</sup>Fe Mössbauer spectroscopy* - For Mössbauer spectroscopic analyses, the remaining liquid samples (ca. 8 ml) were processed  
159 inside an anoxic glove box. The entire liquid including the precipitates was passed through a 0.45 µm filter. The wet filter was



160 then sealed between two layers of Kapton tape and kept inside sealed Schott bottles in a freezer (-20°C) under anoxic conditions  
161 until analysis. From the treatments with DB, samples were collected at day 0 at pH 6.8 and at the end of the experiment (~30  
162 days) for pH 6.8 and 5.8. For the mineral-only experiment, only one sample (time point zero, pH 6.8) was analysed, as a basis  
163 for comparison with the DB experiments (i.e., to verify whether DB has an immediate effect on the mineral phase). Taking  
164 care to minimize exposure to air, samples were transferred from the air-tight Schott bottles and loaded inside a closed-cycle  
165 exchange gas cryostat (Janis cryogenics). Measurements were performed at 77 K with a constant acceleration drive system  
166 (WissEL) in transmission mode with a  $^{57}\text{Co}/\text{Rh}$  source and calibrated against a  $7\mu\text{m}$  thick  $\alpha\text{-}^{57}\text{Fe}$  foil measured at room  
167 temperature. All spectra were analysed using Recoil (University of Ottawa) by applying a Voight Based Fitting (VBF) routine  
168 (Lagarec and Rancourt, 1997; Rancourt and Ping, 1991). The half-width at half maximum (HWHM) was fixed to a value of  
169 0.130 mm/s during fitting.

170 *Nitrite N and O isotope measurements* – The nitrogen (N) and oxygen (O) isotope composition of  $\text{NO}_2^-$  was determined using  
171 the azide method (McIlvin and Altabet, 2005). This method is based on the chemical conversion of  $\text{NO}_2^-$  to gaseous  $\text{N}_2\text{O}$  at a  
172 low pH (4 to 4.5) (McIlvin and Altabet, 2005), and the subsequent analysis of the concentrated and purified  $\text{N}_2\text{O}$  by gas  
173 chromatography— isotope ratio mass spectrometry (GC-IRMS). Addition of 0.6 M NaCl to the acetic acid-azide solution was  
174 conducted in order to minimize oxygen isotope exchange (McIlvin and Altabet, 2005). The acetic acid-azide solution was  
175 prepared freshly every day (McIlvin and Altabet, 2005) and kept in a crimp sealed (grey butyl stopper) 50 ml serum bottle.  
176 Sample volume equivalent to 40 nmol  $\text{NO}_2^-$  was added to pre-combusted headspace vials, filled up to 3 ml with anoxic MilliQ  
177 water, and crimp-sealed. Then, 100  $\mu\text{l}$  of the acetic acid/azide solution was added. After ~7 hrs, 100  $\mu\text{l}$  of 6 M NaOH was  
178 added to stop the reaction. Until isotope analysis by a modified purge and trap gas bench coupled to CF-IRMS (McIlvin and  
179 Casciotti, 2010), the samples were stored upside down in the dark. Nitrite isotope standards (N-7373 and N-10219; Casciotti  
180 & McIlvin, 2007) were prepared on the day of isotope analysis and processed the same way as samples. N and O isotope data  
181 are expressed in the common  $\delta$  notation and reported as per mille deviation (‰) relative to AIR  $\text{N}_2$  and VSMOW, respectively  
182 ( $\delta^{15}\text{N} = ([^{15}\text{N}]/[^{14}\text{N}]_{\text{sample}} / [^{15}\text{N}]/[^{14}\text{N}]_{\text{air-N}_2} - 1) \times 1000\text{‰}$  and  $\delta^{18}\text{O} = ([^{18}\text{O}]/[^{16}\text{O}]_{\text{sample}} / [^{18}\text{O}]/[^{16}\text{O}]_{\text{VSMOW}} - 1) \times 1000\text{‰}$ ).

183  *$\text{N}_2\text{O}$  N and O isotope measurements* – Triplicate 20-nmol samples of  $\text{N}_2\text{O}$  were injected into 20 ml headspace vials that were  
184 flushed before for 5 hrs with 5.0 H<sub>2</sub> injection volumes according to the  $\text{N}_2\text{O}$  concentrations determined before). The  $\text{N}_2\text{O}$  was  
185 then analysed directly using CF-IRMS (see above). Two standard gases with known  $\delta^{15}\text{N}$  and  $\delta^{18}\text{O}$  values were analysed along  
186 with the samples, namely FI.CA06261 ( $\delta^{15}\text{N}$ : -35.74‰,  $\delta^{15}\text{N}^\alpha$ : -22.21‰,  $\delta^{15}\text{N}^\beta$  = -49.28‰,  $\delta^{18}\text{O}$ : 26.94‰) and FI.53504 ( $\delta^{15}\text{N}$ :  
187 48.09‰,  $\delta^{15}\text{N}^\alpha$ : 1.71‰,  $\delta^{15}\text{N}^\beta$  = 94.44‰,  $\delta^{18}\text{O}$ : 36.01‰) (provided by J. Mohn, EMPA; e.g. Mohn et al., 2014). The gases  
188 were calibrated on the Tokyo Institute of Technology scale for bulk and site-specific isotopic composition (Ostrom et al., 2018;  
189 Sakae Toyoda et al., 1999). Ratios of m/z 45/44, 46/44 and the 31/30 signals were used to calculate values of  $\delta^{15}\text{N}^{\text{bulk}}$   
190 (referenced against AIR- $\text{N}_2$ ),  $\delta^{18}\text{O}$  (referenced against V-SMOW), and site-specific  $\delta^{15}\text{N}^\alpha$ ,  $\delta^{15}\text{N}^\beta$  based on Frame and Casciotti  
191 (2010). Site preference (SP) was calculated as  $\delta^{15}\text{N}^\alpha - \delta^{15}\text{N}^\beta$  (Sutka et al., 2006; Toyoda and Yoshida, 1999).

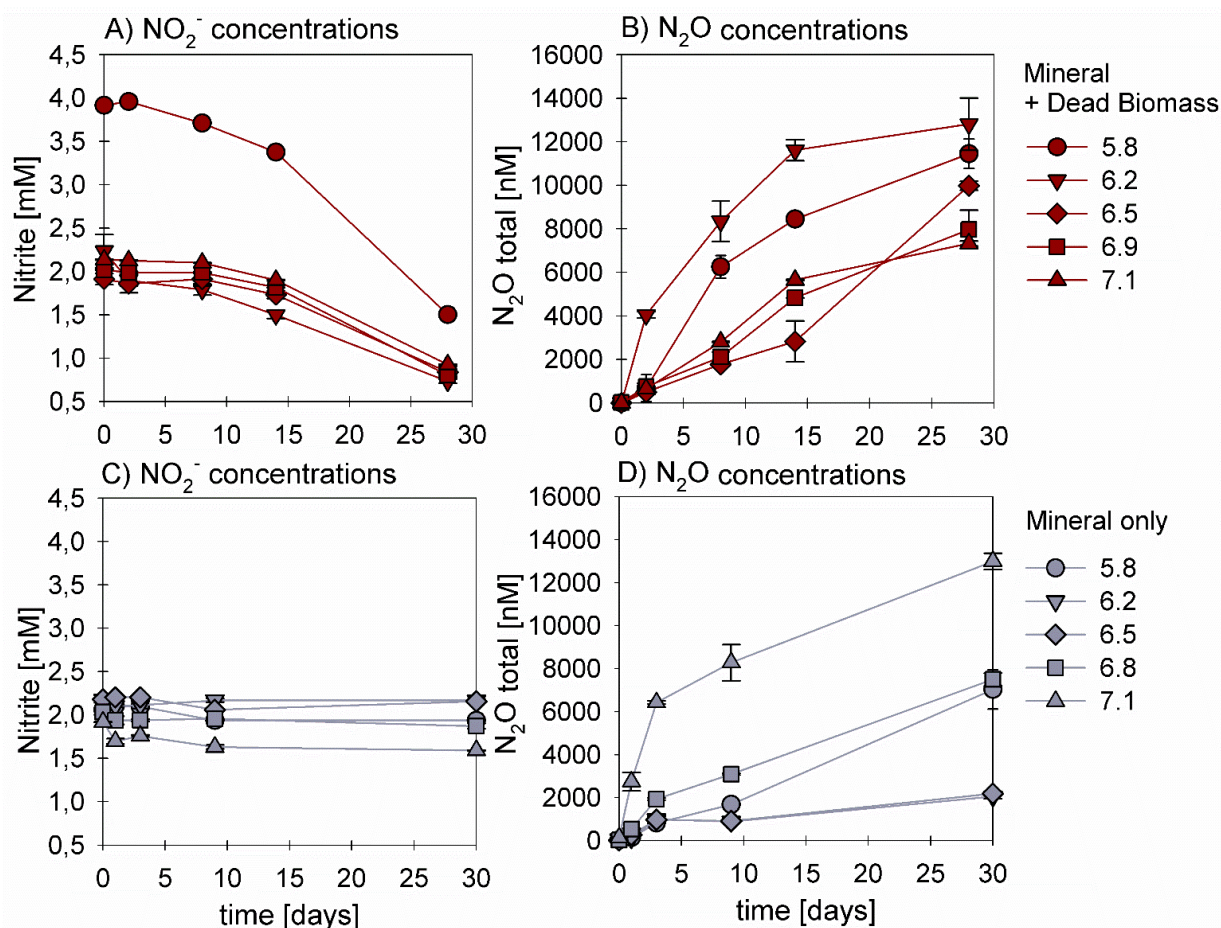


## 192 2.4. Pourbaix diagram

193 In order to predict the stability and behaviour of the N- and Fe(II)-bearing chemical species in the same system, a Pourbaix  
194 (Eh-pH) diagram was constructed (Delahay et al., 1950) as a valuable tool to predict possible reactions and speciation of end  
195 products under different experimental conditions. To calculate the enthalpies for the stepwise reduction of nitrite during  
196 denitrification, as well as Fe(II) oxidation reactions, standard enthalpy values were taken from different references (Table S1).  
197 The Pourbaix diagram presented in the discussion was devised using concentrations measured during the experiments  
198 performed for this study.

## 199 3. Results

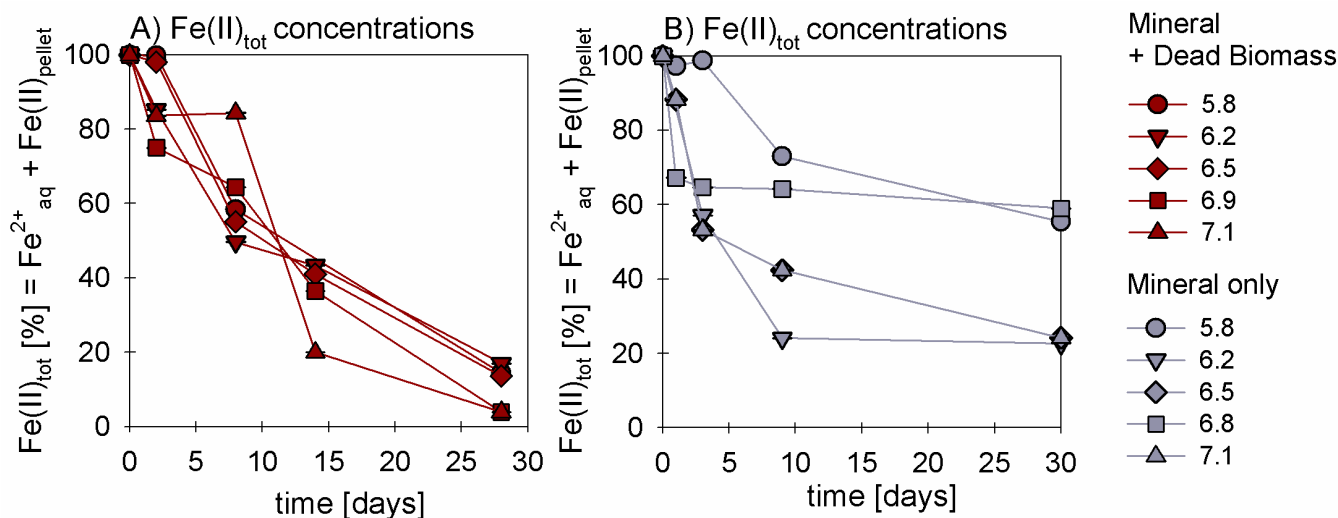
### 200 3.1. Chemodenitrification kinetics



201  
202 **Figure 1: Nitrite reduction (A, C) and N<sub>2</sub>O production (B, D) over time in the mineral + dead biomass (red) and mineral-only (grey)**  
203 **setups over time and at different pH. Please note that at pH 5 twice the amount of nitrite was accidentally introduced. Standard error**  
204 **calculated from biological replicates (n = 9) is represented by the error bars.**



205 In the presence of DB,  $\text{NO}_2^-$  reduction rates were much higher compared to the mineral-only setup (Figure 1 A, C), with up to  
 206 ~60% of the initially amended  $\text{NO}_2^-$  being transformed during the incubation period, independent of the pH. The addition of  
 207 DB led to a decrease in  $\text{NO}_2^-$  concentrations from 2 mM to ~0.7 mM (Figure 1 A). The pH 5.8 treatment (unintentionally  
 208 amended with 2x  $\text{NO}_2^-$ ) also showed a similar fractional reduction. In the mineral-only setups the decrease in  $\text{NO}_2^-$   
 209 concentration was rather moderate and ranged between 0.3 (pH 7) and 0.1 mM (at lower pH) (Figure 1 C). In all treatments,  
 210  $\text{N}_2\text{O}$  was produced but accounted for a maximum of only 0.7% of the  $\text{NO}_2^-$  consumed. The final  $\text{N}_2\text{O}$  yield per mole  $\text{NO}_2^-$   
 211 reduced tended to be lower in the mineral plus DB versus the mineral-only amended setups for most of the pH (Figure 1 B vs.  
 212 D). Highest  $\text{N}_2\text{O}$  production was observed at circumneutral pH (7.1) in the mineral-only setup, while maximum final  $\text{N}_2\text{O}$   
 213 concentrations were observed at lower pH (6.2) in the incubations with DB (Figure 1 B). A systematic pH effect, however,  
 214 could not be discerned.  $\text{Fe(II)}_{\text{total}}$  concentrations rapidly decreased in both setups. In the presence of DB,  $\text{Fe(II)}_{\text{total}}$  oxidation  
 215 was almost complete (Figure 2A), independent of the pH, whereas in the mineral-only experiment,  $\text{Fe(II)}_{\text{total}}$  decreased during  
 216 the first 5-10 days but then seemed to reach a steady state (Figure 2 B). At pH 6.8 and 5.8, only 40% of the  $\text{Fe(II)}_{\text{total}}$  was  
 217 oxidized, whereas at the other pH up to 80% of the  $\text{Fe(II)}_{\text{total}}$  initially amended was oxidized. Total Fe decreased over time  
 218 (Figure S2).



219  
 220 **Figure 2: Oxidation of total Fe(II) over time given (reported as % of initial concentration) in the mineral + dead biomass amended**  
 221 **(red) and the mineral-only setup (grey), tested at different pH. Standard error calculated from biological replicates (n = 9) is**  
 222 **represented by the error bars.**

223  
 224 Average rates for  $\text{NO}_2^-$  reduction and  $\text{N}_2\text{O}$  production at pH 6.8 were calculated (Table 1). Rates were calculated per day and  
 225 again these results emphasize that the amendment of dead biomass increased the rates by ~92%. Although not complete,  $\text{Fe(II)}$   
 226 oxidation in the presence of DB was also more pronounced leading to only  $10.5 \pm 2.8\%$   $\text{Fe(II)}$  remaining compared to the  
 227 mineral-only setup in which  $37.1 \pm 8.2\%$   $\text{Fe(II)}$  remained. To complement the colorimetric data,  $^{57}\text{Fe}$  Mössbauer spectroscopy  
 228 was performed and data are presented in detail in the next section.





229 **Table 1: Chemodenitrification kinetics and mineral transformation during mineral + dead biomass as well as the mineral only**  
 230 **experiments.  $T_{ini}$  values represent means calculated by summarizing results across all pH  $\pm$  standard error. Overall**  
 231 **reduction/production rates are calculated by subtracting  $[\overline{C}]_{t_0} - [\overline{C}]_{t_{end}} \pm \text{standard error} / [\overline{C}]_{t_{end}} - [\overline{C}]_{t_0} \pm \text{standard error}$ ,**  
 232 **respectively and are given per day. Fe(III) values are calculated by using  $^{57}\text{Fe}$  Mössbauer spectroscopy data. Mineral phases were**  
 233 **also identified by using  $^{57}\text{Fe}$  Mössbauer spectroscopy with spectra collected at 77 K. Mineral-only sample taken after 28 days was**  
 234 **inadvertently destroyed prior to Mössbauer measurement.**

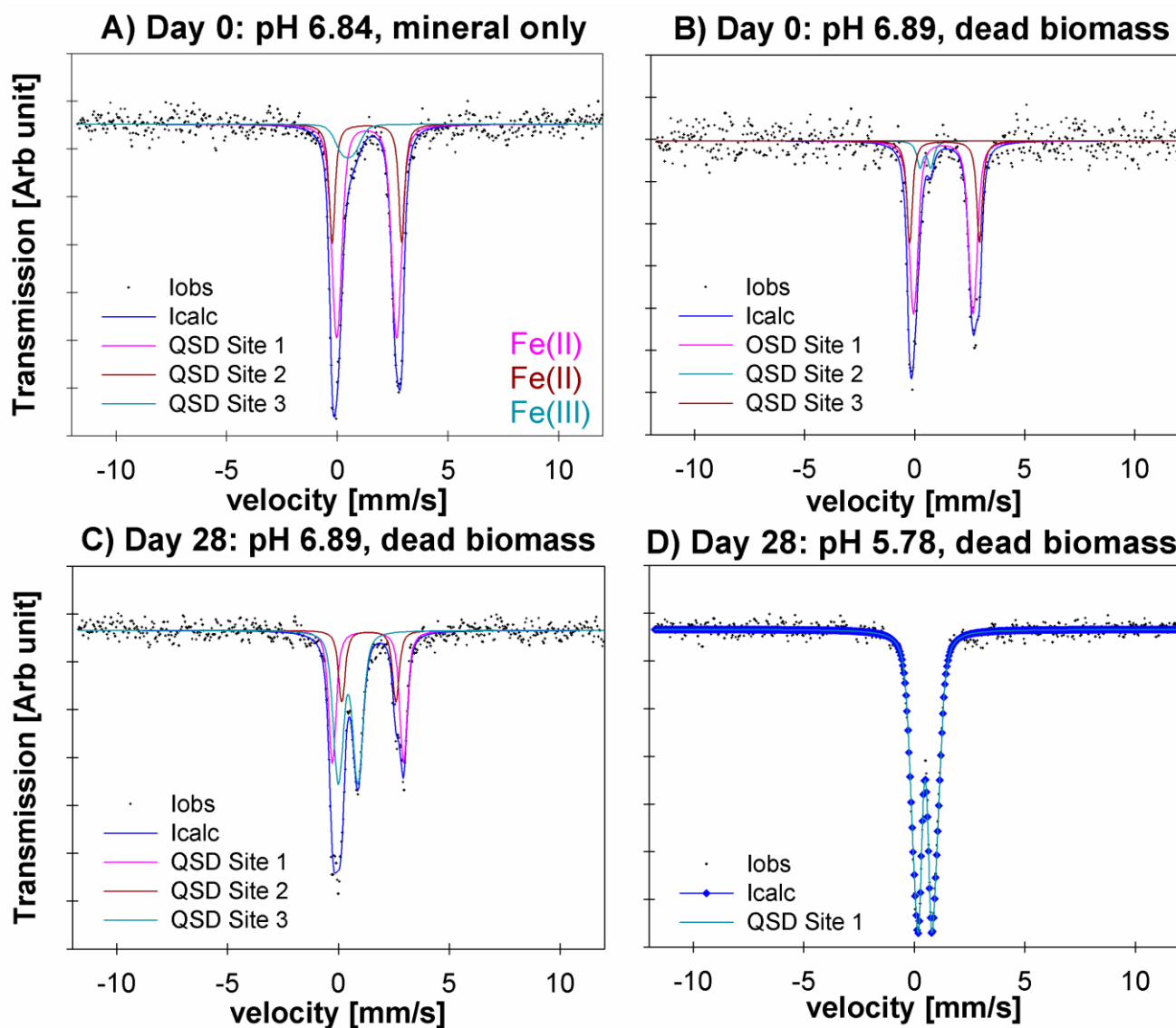
	Mineral + Dead Biomass	Mineral-only
<b>NO<sub>2</sub><sup>-</sup> reduction (<math>\overline{X}</math>)</b>	0.053 $\pm$ 0.013 mmol L <sup>-1</sup> day <sup>-1</sup>	0.004 $\pm$ 0.003 mmol L <sup>-1</sup> day <sup>-1</sup>
<b>N<sub>2</sub>O production (<math>\overline{X}</math>)</b>	353.50 $\pm$ 32.91 nmol L <sup>-1</sup> day <sup>-1</sup>	204.02 $\pm$ 60.29 nmol L <sup>-1</sup> day <sup>-1</sup>
<b>Fe(II)<sub>total</sub> remaining (<math>\overline{X}</math>)</b>	10.54 $\pm$ 2.77%	37.08 $\pm$ 8.23%
<b>Fe(III) after NO<sub>2</sub><sup>-</sup> addition</b>	7.4%	9.9%
<b>Fe(III) after 28 days</b>	48.7%	*
<b>Mineral phase <math>t_{ini}</math></b>	Vivianite	Vivianite
<b>Mineral phase <math>t_{end}</math></b>	Vivianite/Ferrihydrite	*

235 \* Mössbauer sample lost  
 236

### 237 3.2. Fe mineral analysis

238  $^{57}\text{Fe}$  Mössbauer spectroscopy was used to quantify structural Fe(II) and Fe(III) contents of the samples and identify differences  
 239 in mineralogy under the different reaction conditions. The hyperfine parameters of the mineral phases in the mineral-only  
 240 setup at  $t_{initial}$  (pH 6.84) are dominated by Fe(II) doublets (Figure 3 A, QSD Sites 1 and 2), which most closely match that of a  
 241 vivianite spectrum (Muehe et al., 2013; Veeramani et al., 2011). There is a small component with low centre shift and  
 242 quadrupole splitting, indicative of Fe(III), which accounts for ~10% of the spectral area (Figure 3 A, QSD Site 3). This suggests  
 243 some minor oxidation occurred, potentially during transfer of sample into the spectrometer. The mineral phases in the DB-  
 244 amended setup at  $t_{initial}$  (pH 6.89) shows very close approximation to the abiotic mineral-only setup, though with slightly less  
 245 Fe(III) (~7.5% of the spectral area) (Figure 3 B, QSD Site 2). Precipitates analysed at the end of the DB-amended experiment  
 246 (Day 28) show that at pH 6.89, the vivianite phase still dominates (Figure 3 C, QSD Sites 1 and 2), however, the Fe(III)  
 247 component is now much more prominent (Figure 3 C, QSD Site 3), and suggests the formation of a poorly crystalline/short-  
 248 ranged ordered mineral such as ferrihydrite (Cornell and Schwertmann, 2003). At the lowest pH (5.78) and in the presence of  
 249 DB, the pattern of the precipitates is completely dominated by one doublet (Figure 3 C, QSD Site 1), with hyperfine parameters  
 250 corresponding to a poorly ordered Fe(III) mineral such as ferrihydrite (Cornell and Schwertmann, 2003). Unfortunately, the  
 251 mineral-only sample taken after 28 days was lost and can therefore not be used for further elucidations. Detailed fitting results  
 252 of the  $^{57}\text{Fe}$  Mössbauer spectroscopy are provided in Table 2.

253



254

255 **Figure 3:**  $^{57}\text{Fe}$  Mössbauer spectra collected at 77 K for (A) the mineral only setup precipitates at day 0 and pH 6.84, (B) the mineral  
256 + dead biomass amended setup precipitates at day 0 at pH 6.89, (C) the mineral + dead biomass amended setup precipitates at day  
257 28 and (D) the mineral + dead biomass amended setup precipitates at day 28 at pH 5.78. Full lines represent the calculated spectra  
258 and their sums. Colours of the fits represent the corresponding Fe phase and thus vary between the graphs: Fe(II) doublets (A, C –  
259 QSD Sites 1 and 2, B – QSD Sites 1 and 3) closely match the spectra known for vivianite. Minor amounts of Fe(III) are present at  
260 day 0 in both, the mineral-only and DB-amended setups (A/B QSD Site 3/2). Single doublets shown in C (QSD Site 3) and D (QSD  
261 Site 1) correspond to a poorly ordered Fe(III) mineral such as ferrihydrite.

262  
263  
264  
265



266 **Table 2: Fitting results of Mössbauer spectroscopy. CS – centre shift, QS – quadrupole splitting, R.A. – Relative abundance**  
 267 **determined by integration under the curve, Chi<sup>2</sup> – goodness of fit; sample collection took place at t<sub>ini</sub> – initial timepoint and t<sub>end</sub> –**  
 268 **end timepoint; MO = mineral-only, MDB = mineral + dead biomass.**

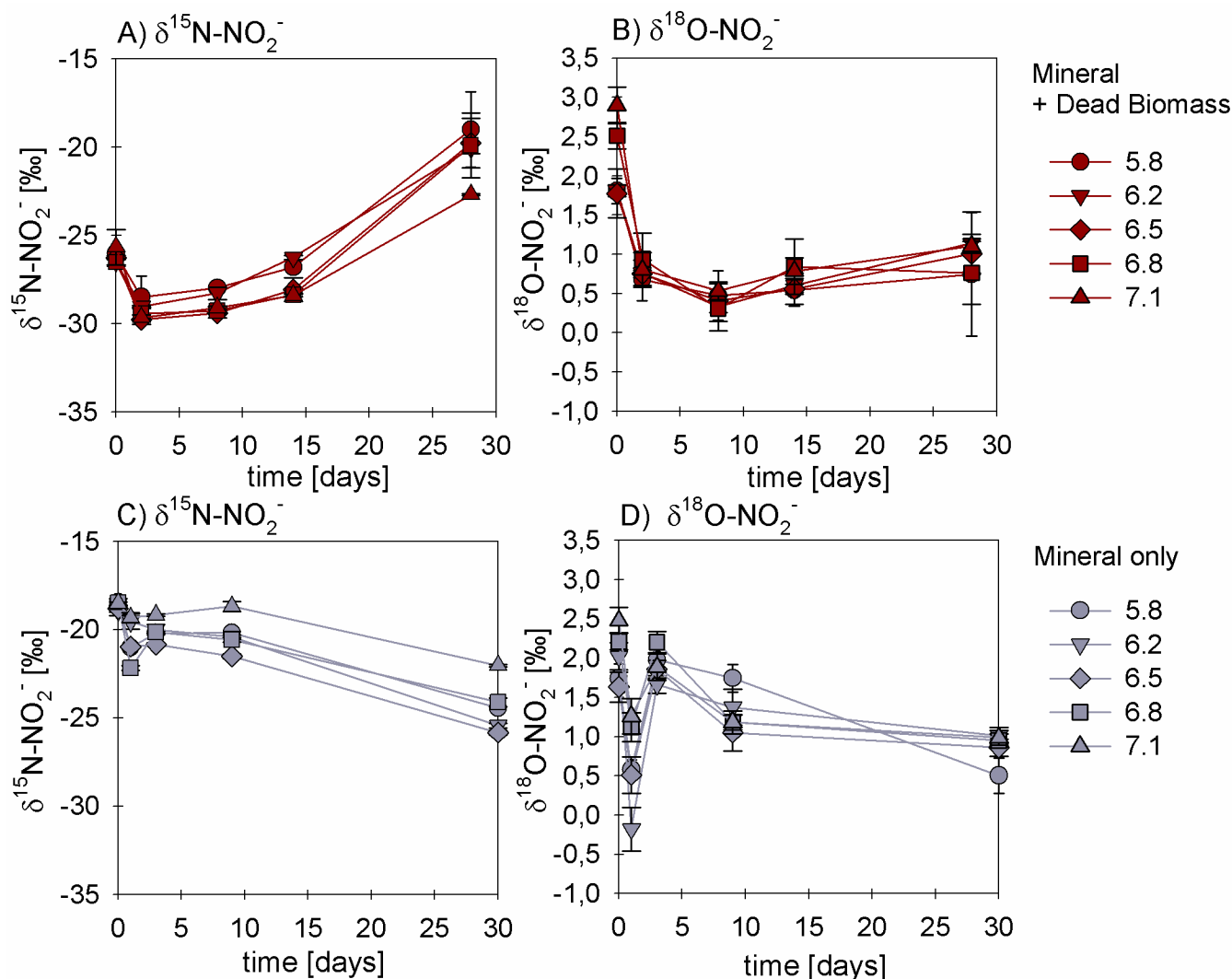
Sample	Temp [K]	Phase	CS [mm/s]	QS [mm/s]	R.A. [%]	Error	Chi <sup>2</sup>
MO_pH6.8_t <sub>ini</sub>	77	Fe(II)	1.32	2.71	66.0	23.0	0.55
		Fe(II)	1.33	3.15	24.0	23.0	
		Fe(III)	0.47	0.63	9.9	4.8	
MDB_pH6.8_t <sub>ini</sub>	77	Fe(II)	1.30	2.70	65.0	14.0	0.68
		Fe(III)	0.49	0.49	7.4	3.6	
		Fe(II)	1.36	3.18	28.0	15.0	
MDB_pH6.8_t <sub>end</sub>	77	Fe(II)	1.33	3.21	34.3	2.4	0.73
		Fe(II)	1.37	2.44	17.0	2.8	
		Fe(III)	0.44	0.89	48.7	2.4	
MDB_pH5.8_t <sub>end</sub>	77	Fe(III)	0.49	0.79	100.0		0.66

269

### 270 3.3. Nitrite and N<sub>2</sub>O isotope dynamics

271 In the experiments with DB, the  $\delta^{15}\text{N-NO}_2^-$  and  $\delta^{18}\text{O-NO}_2^-$  values showed a very consistent initial ~3-4‰-decrease (from -  
 272 26‰ to -30‰ for  $\delta^{15}\text{N}$  and from ~+3‰ to 0‰ for  $\delta^{18}\text{O}$ ) (Figure 4 A, B). After 5 days, the  $\delta^{15}\text{N}$  values started to increase again  
 273 with decreasing  $\text{NO}_2^-$  concentrations, reaching final values of ~ -20‰ (Figure 4 A), whereas the concomitant increase in the  
 274  $\delta^{18}\text{O-NO}_2^-$  was much smaller (<1‰, Figure 4 B). The same pattern was observed for all pH levels. In mineral-only experiments,  
 275 isotope trends were quite different. In combination with far less consumption of  $\text{NO}_2^-$ , the  $\delta^{15}\text{N-NO}_2^-$  values decreased  
 276 throughout the entire abiotic experiment (Figure 4 C). In contrast, the  $\delta^{18}\text{O-NO}_2^-$  first dropped by 2‰, reaching a clear  
 277 minimum of ~-0.5 to -0.5 ‰, before rapidly increasing again. Over the remaining 25 days, the  $\delta^{18}\text{O-NO}_2^-$  slowly decreased  
 278 reaching final values of ~1‰ (Figure 4 D) – similar to that of the DB treatment.

279



280

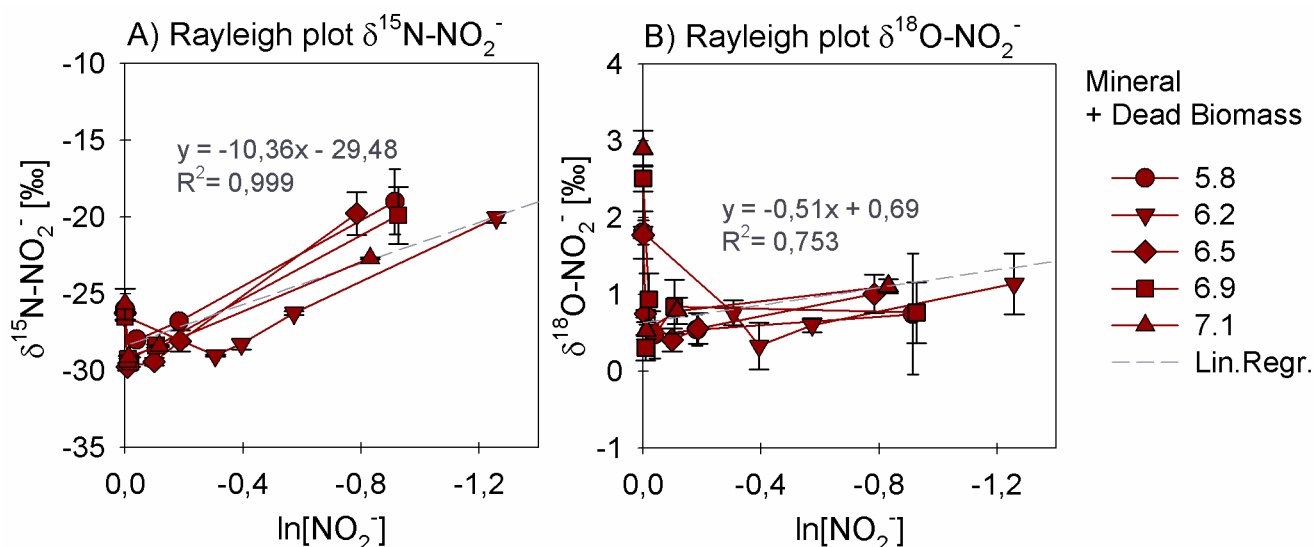
281 **Figure 4:**  $\delta^{15}\text{N}$  (A, C) and  $\delta^{18}\text{O}$  (B, D) values for  $\text{NO}_2^-$  measured in the mineral + dead biomass amended (red) and the mineral-only  
282 (grey) setups over time and at different pH. Standard error calculated from biological replicates (n = 3) is represented by the error  
283 bars.

284

285 In order to estimate the net N and O isotope fractionation for putative  $\text{NO}_2^-$  reduction (in the DB-amended experiments, where  
286 we observed a clear decrease in  $\text{NO}_2^-$ ), we plotted the  $\text{NO}_2^-$   $\delta^{15}\text{N}$  and  $\delta^{18}\text{O}$  values against the natural logarithm of the  
287 concentration of the residual  $\text{NO}_2^-$  (Rayleigh plot), where the slope of the regression line approximates the N and O isotope  
288 effects, respectively (Mariotti et al., 1981). At least after the initial period, when the  $\text{NO}_2^-$   $\delta^{15}\text{N}$  markedly increased with  
289 decreasing  $\text{NO}_2^-$  concentrations, the N isotope data are more or less consistent with Rayleigh isotope fractionation kinetics.  
290 The slope of the regression line suggests an average N isotope effect of -10.4‰ (Figure 5 A). For the mineral-only setup, no  
291 N isotope effect could be calculated, but the observed  $\text{NO}_2^-$   $\delta^{15}\text{N}$  trend suggest a small inverse N isotope fractionation.



292 Similarly, trends in  $\text{NO}_2^-$   $\delta^{18}\text{O}$  of the DB experiments are not as obviously governed by normal Rayleigh fractionation  
293 dynamics, at least not during the initial period, when the  $\delta^{18}\text{O}$  decreased despite decreasing  $\text{NO}_2^-$  concentrations. Considering  
294 the  $\delta^{18}\text{O}$  values only after 2 days of the incubation, the Rayleigh plot revealed an average O isotope enrichment factor of -0.5  
295 ‰ (Figure 5 B), much lower than for N. Similar to N, O-isotope Rayleigh plots for the mineral-only experiments (Figure S4)  
296 did not exhibit coherent trends, as the fractional  $\text{NO}_2^-$  depletion was minor and not consistent (mostly less than 10%). Again,  
297 the observed  $\delta^{18}\text{O}$  minimum at day 2 of the abiotic incubations suggests that processes other than normal kinetic fractionation  
298 during  $\text{NO}_2^-$  reduction were at work, which cannot be described with the Rayleigh model. If at all, the decreasing  $\delta^{18}\text{O}$  values  
299 after day 5 in the mineral-only experiments, accompanying the subtle decrease in  $\text{NO}_2^-$  concentration in at least some of the  
300 treatments, suggest a small apparent inverse O isotope effect associated with the net consumption of  $\text{NO}_2^-$ . Despite the different  
301  $\text{NO}_2^-$   $\delta^{18}\text{O}$  dynamics during the course of the experiment, the final  $\delta^{18}\text{O}$  of the residual nitrite was very similar in both  
302 experimental setups, and independent of the pH.

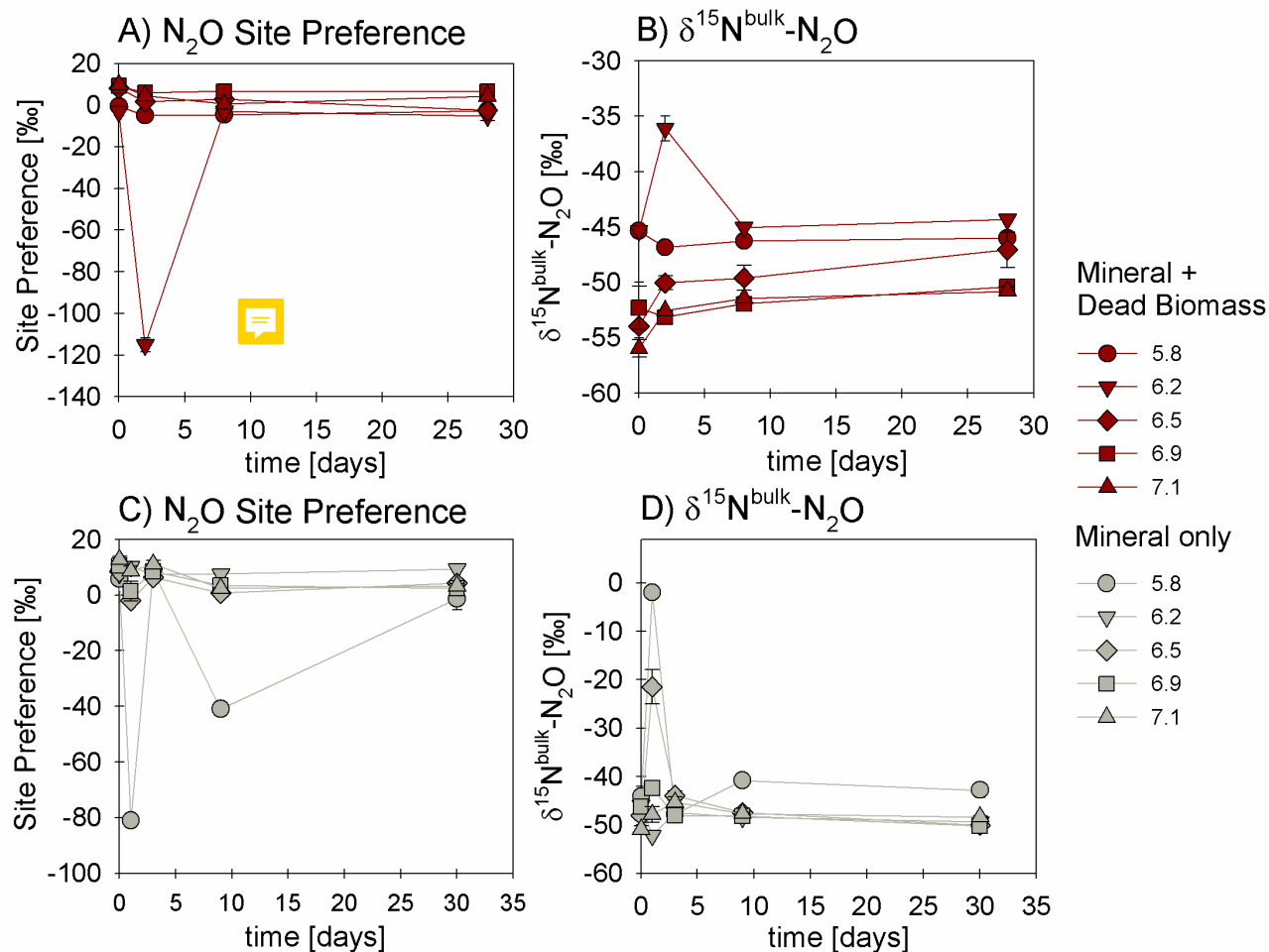


303  
304 **Figure 5: Rayleigh plots for  $\text{NO}_2^-$   $\delta^{15}\text{N}$  (A) and  $\delta^{18}\text{O}$  (B) values measured for the mineral + dead biomass amended setups over the**  
305  **$\ln$  of the substrate fraction remaining and at different pH. The average linear regression line was calculated starting with the lowest**  
306 **delta values (after the initial decrease in both  $\delta^{15}\text{N}$  and  $\delta^{18}\text{O}$  during the initial experimental phase). Equation and  $R^2$  are given in**  
307 **grey. Standard error calculated from biological replicates ( $n = 3$ ) is represented by the error bars.**

308  
309 We also investigated the  $\text{N}_2\text{O}$  isotope dynamics during mineral-only and DB-amended incubations. Site preference and  $\delta^{15}\text{N}^{\text{bulk}}$   
310 of the  $\text{N}_2\text{O}$  produced in both experimental setups were plotted over time (Figure 5 A and B) and show, except for a few values  
311 that require further investigation, almost no variation during the period of the experiment. Also, disregarding the rather high  
312 and unusual (but well replicated) values already mentioned, the majority of values obtained in both setups indicate that neither  
313 pH nor the amendment of DB seems to have had any influence on the isotopic composition of the product  $\text{N}_2\text{O}$  (Figure 5 B vs.



314 D). Over the course of the experiment,  $\delta^{15}\text{N}^{\text{bulk}}$   $\text{N}_2\text{O}$  values were around  $-50\pm 5\%$ . SP was relatively low, ranging between 0  
315 and a maximum of  $+10\%$  (Figure 5A, C), without any significant temporal change.



316

317 **Figure 6: Site Preference (SP; A, C) and  $\delta^{15}\text{N}^{\text{bulk}}$  (B, D) values of  $\text{N}_2\text{O}$  produced in experiments amended with mineral + dead biomass**  
318 **(red) and mineral-only (grey). Standard error calculated from biological replicates ( $n = 3$ , extreme values  $N = 2$ ) is represented by**  
319 **the error bars.**

320

321 Rayleigh diagrams, in which  $\delta^{15}\text{N}^{\alpha}$ ,  $\delta^{15}\text{N}^{\text{bulk}}$  and SP of the  $\text{N}_2\text{O}$  were plotted against concentrations of the reactant ( $\text{NO}_2^-$ )  
322 remaining (Figure S5), confirm the similar  $\text{N}_2\text{O}$  isotope dynamics in the DB vs. mineral-only setups, despite the differential  
323 degree of  $\text{NO}_2^-$  reduction (only minor in the mineral-only experiment, with  $f$  always greater 0.9) and despite the different  $\text{NO}_2^-$   
324 N and O isotope dynamics. Similarly, the dual  $\text{N}_2\text{O}$   $\delta^{18}\text{O}$  vs.  $\delta^{15}\text{N}^{\text{bulk}}$  signatures (with the exception of two data points; Figure  
325 S6) were almost equivalent in both setups, implying that, although modes of  $\text{NO}_2^-$  reduction clearly differ, a similar mechanism  
326 of nitrite-reduction-associated  $\text{N}_2\text{O}$  production exists in both setups. The N and O isotopic results are summarized in Table 3  
327 (see discussion).




## 328 4. Discussion and implications

### 329 4.1. General evaluation of the abiotic reaction systematics

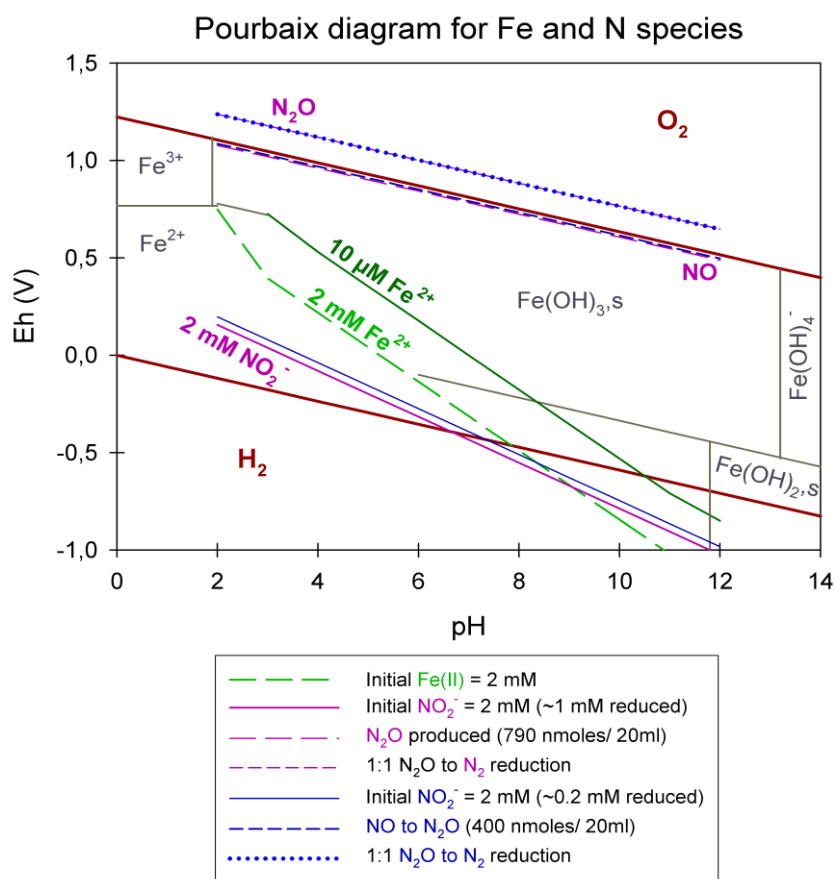
330 Overall, the abiotic reaction between  $\text{NO}_2^-$  and Fe(II), heterogenous or homogenous, has been considered thermodynamically  
331 favourable, and as major contributor to the global  $\text{N}_2\text{O}$  budget (e.g. Jones et al., 2015; Otte et al., 2019). Previous studies on  
332 abiotic  $\text{NO}_2^-$  reduction with Fe(II) have usually been performed in the presence of rather high concentrations ( $>2$  mM) of  $\text{NO}_2^-$   
333 and/or Fe(II), without taking into account that chemodenitrification is in fact considered to be highly concentration-dependent  
334 (Van Cleemput and Samater, 1995). In addition, reaction dynamics were often tested under variable conditions including the  
335 presence of different Fe(II)/Fe(III) minerals, sediments, organic materials and/or bacterial cells (Chen et al., 2018; Grabb et  
336 al., 2017; Otte et al., 2019). Whether  $\text{NO}_2^-$  indeed acts as a direct oxidant of Fe(II) at circumneutral pH or whether the reaction  
337 requires catalysis is still a matter of debate (Kampschreur et al., 2011; Sorensen and Thorling, 1991).

338 Integrating concentrations that are pertinent to our experiments, we constructed a Pourbaix diagram (e.g. Delahay et al., 1950;  
339 Minguzzi et al., 2012) (Figure 7). Based on these (simplified) thermodynamic calculations, the abiotic reaction solely driven  
340 by the reaction of  $\text{NO}_2^-$  and aqueous  $\text{Fe}^{2+}$  at a pH range of 5 to 7 is not supported. Under our experimental conditions,  $\text{Fe}^{2+}$  is  
341 predicted to be oxidized by NO rather than  $\text{NO}_2^-$ . Considering Figure 7, an accumulation of NO at  $\mu\text{M}$  or even mM  
342 concentrations would result in a downward shift of the  $\text{NO}_2^-$  line. Therefore, an accumulation of NO would only lower the  
343 reactivity between  $\text{NO}_2^-$  and  $\text{Fe}^{2+}$ , which implies that  $\text{NO}_2^-$  is not oxidizing  $\text{Fe}^{2+}$ . Again, this also implies that the reactivity  
344 between  $\text{NO}_2^-$  and  $\text{Fe}^{2+}$  is only enhanced if NO concentrations are rather low (pM range). In order to avoid NO accumulation  
345 and thus to enhance the abiotic reaction between  $\text{NO}_2^-$  and  $\text{Fe}^{2+}$ , NO would need to react further (either with  $\text{Fe}^{2+}$  or otherwise).

346 This would induce a reaction cascade, resulting in the constant reduction of  $\text{NO}_2^-$  and NO, and thus in higher  $\text{N}_2$    
347 concentrations. In contrast, if NO does accumulate as previously reported, the reaction between  $\text{NO}_2^-$  and  $\text{Fe}^{2+}$  would be  
348 suppressed and only NO could be reduced further to  $\text{N}_2\text{O}$ , a reaction that of course also depends on gas equilibration dynamics  
349 occurring with the headspace of the system. Nevertheless, considering all these aspects, including the fact that the  $\text{N}_2\text{O}$   
350 produced corresponds only to a minor fraction of the initial  $\text{NO}_2^-$  reduced, NO acting as main oxidizing agent seems more  
351 likely. The reaction mechanisms in this system are, however, complex and we note that this simplified thermodynamic analysis  
352 does neglect catalytic effects that are possibly induced by reactive surfaces. The complexity of this system is further indicated  
353 by the fact that, according to the Pourbaix diagram, a pH response towards  $\text{N}_2\text{O}$  accumulation would be expected which has,  
354 however, never been reported so far. Furthermore, testing various pH did not reveal an obvious pH effect on the reaction  
355 dynamics. Changes in pH will most certainly affect interactions between species such as HNO,  $\text{NO}_2$  and  $\text{N}_2\text{O}$  and thus could  
356 impact the reaction dynamics. In addition, the results observed in the setup biased by accidentally adding twice as much  $\text{NO}_2^-$   
357 (DB, pH 5.8) do not differ from the results of the other setups and thus might question the previously mentioned concentration  
358 dependency (i.e.  $[\text{NO}_2^-]$ ). It appears that, for a more detailed understanding of this redox system, the reactants/intermediates  
359 involved and thus the specific reaction kinetics would need to be determined. Unfortunately, quantification of these  
360 intermediates is hampered by their high reactivity, transient nature, and lack of detection techniques that can be applied in



361 batch culture experiments. Since low amounts (e.g.,  $\mu\text{M}$ ) of  $\text{NO}$  suffice to impact reaction dynamics and thus stimulate the  
 362 reaction between  $\text{NO}_2^-$  and  $\text{Fe}^{2+}$ ,  $\text{NO}$  quantification could be crucial to assess the environmental controls on  $\text{Fe(II)}$ -coupled  
 363 chemodenitrification. In laboratory biological denitrification experiments, accumulation of  $\text{NO}$  has been reported (Goretski  
 364 and Hollocher, 1988; Zumft, 1997) and was shown to even account for up to 40% of the initial  $\text{NO}_3^-$  amended (Baumgärtner  
 365 and Conrad, 1992; Choi et al., 2006; Kampschreur et al., 2011; Ye et al., 1994; Zumft, 1997). Hence, Kampschreur et al.,  
 366 (2011) concluded that chemodenitrification is not necessarily solely caused by a single-step reaction, and proposed that the  
 367 oxidation of  $\text{Fe}^{2+}$  is rather caused by a two-step mechanism. They observed an immediate formation and accumulation of  $\text{NO}$   
 368 after  $\text{NO}_2^-$  was added to  $\text{Fe}^{2+}$ , and as soon as a considerable fraction of the  $\text{Fe}^{2+}$  was oxidized,  $\text{N}_2\text{O}$  formation was detected.  
 369 Although  $\text{NO}$  and other possible intermediate (e.g.  $\text{NO}_2(\text{g})$ ) concentrations might not play a major role with regard to mass  
 370 balance considerations, their possible impact on the overall reaction systematics as well as the isotopic fractionation, remains  
 371 unclear.



372  
 373 **Figure 7: Pourbaix diagram depicting an Fe and N-species based system. Overall calculations are based on the Nernst equation using**  
 374 **values taken from literature (for equation and values see table S1). Green lines represent  $\text{Fe}^{2+}$  concentrations, pink lines represent**  
 375  **$\text{NO}_2^-$  reduction experiments, starting with 2 mM  $\text{NO}_2^-$ , resulting in the reduction of 1 mM  $\text{NO}_2^-$ , the production of 790 nmol /20 ml**  
 376  **$\text{N}_2\text{O}$  and a 1:1 transformation of  $\text{N}_2\text{O}$  to  $\text{N}_2$ ; blue lines represent  $\text{NO}_2^-$  reduction experiments, starting with 2 mM  $\text{NO}_2^-$ , resulting in**  
 377 **the reduction of 0.2 mM  $\text{NO}_2^-$ , the production of 790 nmol /20 ml  $\text{N}_2\text{O}$  and a 1:1 transformation of  $\text{N}_2\text{O}$  to  $\text{N}_2$ . Reduction/production**  
 378 **values were taken from our results presented in 3.1.**





#### 379 4.2. Surface catalysis of chemodenitrification

380 Previous studies have shown that the initial presence of either Fe(III)(oxyhydr)oxides (Coby & Picardal, 2005; Klueglein &  
381 Kappler, 2013; Sorensen & Thorling, 1991) or amorphous Fe(II) minerals (Van Cleemput and Samater, 1995) can stimulate  
382 the abiotic reaction between  $\text{NO}_2^-$  and  $\text{Fe}^{2+}$ . As summarized in Table 1, under mineral-only conditions  $\text{NO}_2^-$  reduction was  
383 significantly lower ( $0.004 \pm 0.003 \text{ mmol L}^{-1} \text{ day}^{-1}$ ) than in identical experiments containing DB, which substantially enhanced  
384  $\text{NO}_2^-$  reduction ( $0.053 \pm 0.013 \text{ mmol L}^{-1} \text{ day}^{-1}$ ). The catalytic effect of Fe minerals on the abiotic  $\text{NO}_2^-$  reduction, which has  
385 been demonstrated before, seems to be amplified in the presence of DB. Relative to  $\text{NO}_2^-$  reduction rates, overall final  $\text{N}_2\text{O}$   
386 yields per mole  $\text{NO}_2^-$  reduced tended to be higher in the mineral-only setups. However, considering the initial  $\text{NO}_2^-$   
387 concentrations, only minor amounts of  $\text{N}_2\text{O}$  were produced in both setups, raising questions about the contribution of  
388 chemodenitrification to global  $\text{N}_2\text{O}$  emissions discussed by others (Grabb et al., 2017; Jones et al., 2015; Otte et al., 2019). For  
389 example, in comparison to the  $\text{N}_2\text{O}$  yields in experiments where chemodenitrification was catalysed by green rust (up to 31%,  
390 Grabb et al., 2017), the amount of  $\text{N}_2\text{O}$  produced in our setups is far lower (<5% of the initial  $\text{NO}_2^-$ ).

391 Fe-bearing minerals are known for their high reactivity, ability to complex ligands (metals, humics) and phosphates, and  
392 surface protonation capacity via the sorption of  $\text{OH}^-$  groups (Elsner et al., 2004; Stumm and Sulzberger, 1992). Surface  
393 catalytic effects may include *direct* and *indirect* sorption-induced catalysis. In the environment, pH has been shown to have a  
394 strong influence on these sorption capacities of Fe minerals in general (Fowle and Konhauser, 2011). Considering the point of  
395 zero charge (PZC) of vivianite, which is with 3.3 below the lowest tested pH in our experiments, the mineral surface is  
396 positively charged under our experimental conditions (Luna-Zaragoza et al., 2009). Hence the pH range tested here will not  
397 affect the surface charge, and  $\text{NO}_2^-$  sorption onto mineral surfaces and corresponding heterogeneous reactions are possible. In  
398 contrast, cell surfaces are considered to be negatively charged (Wilson et al., 2001) and therefore might induce different effects  
399 than mineral surfaces. The charge of the cell surface most likely remained negative even after autoclaving (see e.g. Halder et  
400 al., 2015). Our results imply that the systematics of chemodenitrification are strongly dependent on the surface provided and  
401 that, depending on the availability and quality of catalytic surfaces, Fe coupled chemodenitrification may be a single-step  
402 reaction (between  $\text{NO}_2^-$  and Fe) or may occur in multiple steps (reaction between Fe and  $\text{NO}_2$ , as well as Fe and NO). As a  
403 consequence, the nature of surface catalysis would likely have a strong impact on the  $\text{N}_2\text{O}$  yield per mole  $\text{NO}_2^-$  reduced to NO.  
404 Since NO has been demonstrated to have a rather exceptional affinity towards  $\text{Fe}^{2+}$  and  $\text{Fe}^{3+}$  centres resulting in the formation  
405 of  $\text{Fe}^{x+}(\text{NO})_n$  nitrosyls and thus triggering an enhancement of the  $\text{N}_2\text{O}$  decomposition rate (e.g. Rivallan et al., 2009). It remains  
406 unclear to what extent, and why, the quality of the catalytic surfaces plays a role. Particularly in the presence of organics and/or  
407 dead bacterial cells, which are known to have a high affinity to bind metal ions (e.g.  $\text{Ni}^{2+}$ ,  $\text{Cu}^{2+}$  or  $\text{Zn}^{2+}$ ), either directly or by  
408 forming surface complexes with hydroxyl groups (Fowle and Konhauser, 2011), a surface-catalysis-induced reaction can be  
409 expected. Besides acting as a catalyst via a reactive surface, the dead biomass might also have directly triggered the reaction.  
410 For example, non-enzymatic NO formation was studied and modelled by Zweier et al. (1999), suggesting that at concentrations  
411 between 100 and 1000  $\mu\text{M}$ , abiotic  $\text{NO}_2^-$  disproportionation and thus NO formation at circumneutral pH in organic tissue is



412 still possible (Zweier et al., 1999). Furthermore, autoclaving might have ruptured cell walls and released organic compounds.  
413 In the presence of phenolic compounds, humic substances, and other organic compounds,  $\text{NO}_2^-$  has been shown to form NO  
414 via self-decomposition (Nelson and Bremner, 1969; Stevenson et al., 1970; Tiso and Schechter, 2015). Whether this may have  
415 been the case also in our experiments remains unclear, since we did not conduct experiments containing only DB and  $\text{NO}_2^-$ .  
416 Another possible consideration is the presence of extracellular polymeric substances (EPS), which should also be tested in  
417 future studies. Liu et al., (2018) investigated nitrate-dependent Fe(II) oxidation with *Acidovorax* sp. strain BoFeN1, showing  
418 that *c*-cytochromes were present in EPS secreted which could indeed act as electron shuttling agents involved in electron  
419 transfer supporting chemolithotrophic growth. Since *S. oneidensis*, our model organisms used as DB supply, is known to  
420 produce large amounts of EPS, harbouring *c*-cytochromes (Dai et al., 2016; Liu et al., 2012; White et al., 2016), a potential  
421 impact of EPS on the reaction between  $\text{NO}_2^-$  and Fe(II) needs to be considered. However, possible cytochromes present in the  
422 EPS most likely lost their activity due to protein denaturation during autoclaving (Liu & Konermann, 2009; Tanford, 1970).  
423 Nevertheless, EPS is still present and can act as a catalysing agent to the abiotic reaction mechanism (Klueglein et al., 2014;  
424 Nordhoff et al., 2017).  
425 Fe(II)<sub>total</sub> oxidation via  $\text{NO}_2^-$  has also been observed in the mineral-only setups, but to a lower extent. Hence, the vivianite  
426 mineral surfaces themselves seem to catalyse the abiotic reaction between  $\text{NO}_2^-$  and Fe(II)/  $\text{Fe}^{2+}$  (in parts, the stimulation of  
427 Fe-dependent nitrite reduction may also be attributed vivianite dissolution providing ample Fe(II) substrate). Previous studies  
428 reported on mineral-enhanced chemodenitrification (Dhakal et al., 2013; Grabb et al., 2017; Klueglein & Kappler, 2013;  
429 Rakshit et al., 2008), and the catalytic effect may be due to  $\text{NO}_2^-$  adsorption onto the minerals surface possibly facilitating a  
430 direct electron transfer. Similar findings have been reported previously on Fe(II) oxidation promoted by electron transfer  
431 during adsorption onto a Fe(III) minerals surface (Gorski and Scherer, 2011; Piasecki et al., 2019).  $\text{OH}^-$  adsorption is probably  
432 enabled by the minerals positive surface charge at  $\text{pH} > 6$ , resulting in a limited reactive surface availability. Complexation of  
433 dissolved  $\text{Fe}^{2+}$ , which is provided by mineral dissolution, by  $\text{OH}^-$  groups would thus result in a lower overall  $\text{NO}_2^-$  reduction  
434 rate compared to the DB-amended setups. Nevertheless, the NO formed by the initial  $\text{NO}_2^-$  reduction could, at still elevated  
435  $\text{Fe}^{2+}$  levels, proceed until both dissolved and adsorbed Fe(II) is quantitatively oxidized to surface-bound Fe(III) (Kampschreur  
436 et al., 2011). This would ultimately lead to similar Fe(II)<sub>total</sub> oxidation and  $\text{N}_2\text{O}$  production (and thus higher  $\text{N}_2\text{O}$  yields) as in  
437 the DB amended experiment and thus explain the similar results.

### 438 4.3. Mineral alteration during Fe-coupled chemodenitrification

439 We used  $^{57}\text{Fe}$  Mössbauer spectroscopy in order to determine, whether the catalytic effects that enhanced chemodenitrification  
440 with  $\text{Fe}^{2+}$  also modulated mineral formation. In both setups, addition of  $\text{Fe(II)Cl}_2$  to the 22 mM bicarbonate buffered medium  
441 led to the formation of vivianite, an Fe(II)-phosphate. Shortly after the addition of  $\text{Fe}^{2+}_{\text{aq}}$ , the mineral phase in both setups was  
442 dominated by Fe(II), but a small fraction of Fe(III) was also present. Initial fractions of Fe(III) were similar in both the mineral-  
443 only and DB-amended experiments (9.9% and 7.4%, respectively) and, if not an artefact of Mössbauer sample handling, might  
444 therefore have stimulated Fe(II) adsorption and oxidation (Gorski and Scherer, 2011; Piasecki et al., 2019). The reduction of



445  $\text{NO}_2^-$  was accompanied by a marked increase of Fe(III), likely in the form of short-range ordered ferrihydrite or lepidocrocite.  
446 Thus, the Fe(III) phase detected at day 0 most likely formed immediately after  $\text{NO}_2^-$  addition. This is supported by prior studies,  
447 which demonstrated the initiation of Fe(II) oxidation with  $\text{NO}_2^-$  within a short period of time (Jamieson et al., 2018; Jones et  
448 al., 2015). At the end of the DB experiment at pH 6.89, oxidized Fe(III) (most likely in the form of poorly ordered ferrihydrite)  
449 contributed 48.7% to the total Fe phases, with vivianite accounting for the remaining spectral area. Unfortunately, we are  
450 unable to compare the results of the DB-amended precipitates at the end of the experiment to the mineral-only setup, since the  
451 sample was lost. In contrast to our observations, other studies conducted in the presence of organics have identified goethite  
452 as the main Fe(III) phase during the abiotic reaction between Fe(II) and  $\text{NO}_2^-$  (Chen et al., 2018; Liu et al., 2018). In NDFeO  
453 experiments, the formation of lepidocrocite, goethite, hematite and to some extent, magnetite has been reported (e.g. Klueglein  
454 et al., 2014; Liu et al., 2018; Miot et al., 2015). In contrast, minerals obtained from the enrichment culture KS were mostly  
455 vivianite and ferrihydrite, which is, however, attributed to the fact that for the cultivation of the KS culture a high-phosphate  
456 medium is used (Nordhoff et al., 2017). In the abiotic experiments (10 mM Fe(II) and 10 mM  $\text{NO}_2^-$ ) presented by Jones et al.,  
457 (2015), the formation of lepidocrocite, goethite and two-line ferrihydrite were observed after 6 to 48 hrs. In the experiments  
458 presented here, besides a short-range ordered Fe(III) phase, likely ferrihydrite, no other mineral phases could be identified  
459 after 28 days.

460 Iron analysis also indicates that the oxidation of the  $\text{Fe(II)}_{\text{total}}$  went to completion at pH 5.8 whereas at pH 6.8, 52.3% of the  
461  $\text{Fe(II)}_{\text{total}}$  remained at the end of the incubation experiment, resulting in the formation of a poorly-ordered ferrihydrite.  
462 Unfortunately, we did not measure the zeta potential of the starting solutions, which would probably help to explain the  
463 differences detected. We note that, although  $^{57}\text{Fe}$  Mössbauer spectroscopy was used to measure the Fe(II)/Fe(III) in the  
464 precipitates, the reported  $\text{Fe(II)}_{\text{total}}$  concentrations reflect the total Fe(II), i.e., of both the dissolved pellet (structurally-bound  
465 or adsorbed) and the aqueous  $\text{Fe}^{2+}$  in the supernatant measured by Ferrozine. The results obtained by Mössbauer analysis (50%  
466 Fe(II) remaining) seem to contradict the ferrozine assay (<10% remaining) (see Table 1 and 2). The presence of ferrous Fe,  
467 either as structurally-bound Fe(II) or adsorbed  $\text{Fe}^{2+}$  does indeed play a crucial role with regards to the reaction dynamics  
468 occurring at the mineral surfaces, particularly if we assume that N-reactive species are also still present (Rivallan et al., 2009).  
469 In addition, the initially formed Fe(III) phase might also induce another feedback to the N and even the Fe cycle since Fe(III)  
470 minerals are also highly reactive (Grabb et al., 2017; Jones et al., 2015). Mineral structure and thus Fe(II) location within the  
471 lattice can influence the overall Fe accessibility, the binding site at the mineral surface and thus overall reactivity (Cornell and  
472 Schwertmann, 2003; Luan et al., 2015; Schaefer, 2010). If the initial formation of Fe(III), however, enhanced the reaction  
473 between  $\text{NO}_2^-$  and Fe(II), similar results in both setups should have been observed, which this was not the case since  $\text{NO}_2^-$   
474 reduction patterns in the mineral-only experiments were much lower. This also indicates again, that the presence of DB indeed  
475 contributed greatly to the reaction in the DB experiments. Furthermore, results obtained from Mössbauer analysis are the only  
476 results supporting a pH-dependent effect: At pH 5.78 and in the presence of DB, all vivianite was fully transformed into a  
477 short-range ordered Fe(III) phase whereas at pH 6.89, vivianite remained a major component. This presence of vivianite also  
478 indicates that no further Fe(II) oxidation occurred even though  $\text{NO}_2^-$  reduction was incomplete. The incomplete reduction of



479  $\text{NO}_2^-$  in turn suggests that further Fe(II) oxidation was limited due to blocked or deactivated reaction sites on mineral surfaces.  
480 Also, considering that at pH 5.8 and in the presence of DB, the initial  $\text{NO}_2^-$  concentrations were higher but the overall reaction  
481 dynamics were quite similar to the other reaction conditions, the concentration dependency of the reaction between  $\text{NO}_2^-$  and  
482 Fe(II) is again supported.

#### 483 4.4. Nitrite and $\text{N}_2\text{O}$ N and O isotope dynamics during chemodenitrification

484 In the presence of only vivianite, a decrease in  $\delta^{15}\text{N}\text{-NO}_2^-$  of  $\sim 3\text{‰}$  was observed with the initial decrease in  $\text{NO}_2^-$ . Initial  $\delta^{18}\text{O}\text{-}$   
485  $\text{NO}_2^-$  values also reflect this drop of  $3\text{‰}$  during the first 3 days but level off and stabilize at  $1\text{‰}$  after 9 days. The initial decrease  
486 in both  $\delta^{15}\text{N}$  and  $\delta^{18}\text{O}$  of  $\text{NO}_2^-$  suggest apparent inverse isotope effects, which to the best of our knowledge have never been  
487 observed during chemodenitrification, and have only been reported for enzymatic  $\text{NO}_2^-$  oxidation (Casciotti, 2009). Since  
488 biological  $\text{NO}_2^-$  oxidation can be ruled out (no  $\text{NO}_3^-$  produced, no microbes), the decrease in  $\delta^{15}\text{N}\text{-NO}_2^-$ , though subtle, could  
489 indicate that either heavy isotopes are incorporated in the products formed (i.e.  $\text{NO}$ ,  $\text{N}_2\text{O}$ ), at least at the beginning of the  
490 incubation period. Normally, the heavier isotopes build compounds with molecules of higher stability (Elsner, 2010; Fry, 2006;  
491 Ostrom & Ostrom, 2011). This is particularly true for the formation of some minerals or highly stable molecules that are  
492 formed under mineral-only conditions, where processes can reach an isotopic equilibrium (He et al., 2016; Hunkeler & Elsner,  
493 2009; Li et al., 2011; Ostrom & Ostrom, 2011). However, in the system presented here, N incorporation into mineral phases  
494 can be excluded, hence another process must favour the heavy N-atoms. Since this initial drop in  $\delta^{15}\text{N}$  was also observed in  
495 the DB-amended experiments, a possible explanation might be that the isotope values here reflect the sorption or complexation  
496 mechanism of  $\text{NO}_2^-$  onto the reactive surfaces. In contrast  $\delta^{18}\text{O}\text{-NO}_2^-$  values, after the initial decrease, did not change greatly  
497 with decreasing  $\text{NO}_2^-$  concentrations. The stabilization of the  $\delta^{18}\text{O}\text{-NO}_2^-$  towards the end of the experiment most likely reflects  
498 the oxygen isotope equilibration between  $\delta^{18}\text{O}\text{-NO}_2^-$  and the  $\delta^{18}\text{O}$  of the water in the medium. Temporal  $\delta^{18}\text{O}\text{-NO}_2^-$  dynamics  
499 did not change greatly between the different pH treatments, and in all cases the final  $\delta^{18}\text{O}\text{-NO}_2^-$  ranged between  $0.5$  and  $1\text{‰}$ .  
500 The kinetics of abiotic O-atom exchange is a function of temperature and pH. At near neutral pH, at room temperature, one  
501 can expect  $\text{NO}_2^-$  to be fully equilibrated after two to three days (Casciotti et al., 2007). At higher pH, the first order rate  
502 constants for the equilibration with water are lower (Buchwald and Casciotti, 2013), but equilibrium conditions should have  
503 been reached well within the incubation period. Indeed, the final  $\delta^{18}\text{O}\text{-NO}_2^-$  was consistent with an equilibrium O isotope effect  
504 between  $\text{NO}_2^-$  and  $\text{H}_2\text{O}$  with a  $\delta^{18}\text{O}$  of  $\sim -11.5\text{‰}$  (Buchwald and Casciotti, 2013). With regards to  $\delta^{15}\text{N}\text{-NO}_2^-$  values of the DB-  
505 amended experiments, a similar behaviour is found within the first 3 days (i.e., decrease in  $\delta^{15}\text{N}$ ), followed by a clear increase  
506 in  $\delta^{15}\text{N}\text{-NO}_2^-$  of  $\sim 10\text{‰}$ . While it is difficult to explain the initial decrease in  $\delta^{15}\text{N}\text{-NO}_2^-$  (a feature that was not observed in other  
507 chemodenitrification experiments (i.e. Grabb et al., 2017; Jones et al., 2015), the subsequent increase in  $\delta^{15}\text{N}$  can be attributed  
508 to normal isotopic fractionation associated with chemodenitrification and an N isotope effect ( $-9\text{‰}$ ) that is consistent with  
509 those previously reported on Rayleigh-type N and O isotope kinetics during chemodenitrification with Fe(III)-bearing minerals  
510 such as nontronite and green rust (Grabb et al., 2017). In contrast,  $\delta^{18}\text{O}\text{-NO}_2^-$  values initially decrease as in the abiotic  
511 experiment but then level off faster reaching final values of  $\sim 1\text{‰}$ , again most likely explained by O atom isotope exchange



512 pulling the  $\delta^{18}\text{O}-\text{NO}_2^-$  values towards the O-isotope equilibrium value. This value is given by the  $\delta^{18}\text{O}_{\text{H}_2\text{O}} + {}^{18}\epsilon_{\text{eq,NO}_2^-}$ , whereas  
513 the latter is defined as the equilibrium isotope effect between  $\text{NO}_2^-$  and  $\text{H}_2\text{O}$  and has been shown to yield values of roughly  
514  $+13\%$  (Casciotti et al., 2007). Overall, it seems that the non-linear behaviour of the  $\text{NO}_2^-$  in the O isotope Rayleigh plot is most  
515 likely due to the combined effects of kinetic O isotope fractionation during  $\text{NO}_2^-$  reduction, and O atom exchange between  
516  $\text{NO}_2^-$  and  $\text{H}_2\text{O}$ .

517  $\text{NO}_2^-$  N and O isotope trends observed under the DB-amended conditions (in which a large portion of the  $\text{NO}_2^-$  pool was  
518 consumed), somewhat contradict prior reports of chemodenitrification exhibiting a clear increase in both  $\delta^{15}\text{N}$  and  $\delta^{18}\text{O}-\text{NO}_2^-$ ,  
519 with N isotope enrichment factors for  $\text{NO}_2^-$  reduction between  $-12.9$  and  $-18.1\%$  and an O isotope effect of  $-9.8\%$  (Jones et  
520 al., 2015). Consistent with our data, however, they also observed that, at least in abiotic experiments where  $\text{NO}_2^-$  consumption  
521 is rather sluggish due to  $\text{Fe}^{2+}$  limitation (as a result of either oxidation or simply occlusion), O-isotope exchange isotope effects  
522 mask the effects of kinetic O isotope fractionation. While we cannot say at this point what exactly governs the combined  $\text{NO}_2^-$   
523 N vs. O isotope trends in the two different experimental conditions, we observed that the two processes (water isotope  
524 equilibrium and KIE) competing with each other lead to different net dual isotope effects. Our data cannot resolve whether  
525 these observations reflect fundamental differences or simply changes in the relative proportion of the competing processes.  
526 Nevertheless, our observations may still be diagnostic for chemodenitrification catalysed by a mineral surface on the one hand,  
527 and Fe-coupled chemodenitrification that involves catalytic effects by dead bacterial cells on the other. The mineral catalyst  
528 evidently plays an important role with regards to chemodenitrification kinetics, reaction conditions, surface complexation or  
529 contact time between the  $\text{NO}_2^-$  substrate and the mineral phase (Samarkin et al., 2010), and in turn the combined  
530 kinetic/equilibrium N and O isotope effects.

531 The  $\Delta^{15}\text{N}$  values ( $\Delta^{15}\text{N} = \delta^{15}\text{N}_{\text{nitrite}} - \delta^{15}\text{N}_{\text{N}_2\text{O}^{\text{bulk}}}$ ) presented in Table 3 were obtained by subtracting the average  $\delta^{15}\text{N}^{\text{bulk}}$  value of  
532  $\text{N}_2\text{O}$  (abiotic  $-46.5 \pm 0.2\%$ ; dead biomass  $-49.4 \pm 1.0\%$ ) across all pH and throughout the experiment from the average of the  
533 initial  $\delta^{15}\text{N}_{\text{nitrite}}$  value. These values can provide insight on reaction kinetics between  $\text{NO}_2^-$ ,  $\text{NO}$ , and  $\text{N}_2\text{O}$  (Jones et al., 2015).  
534 In both setups there is an offset between the  $\text{NO}_2^-$  and  $\text{N}_2\text{O}$   $\delta^{15}\text{N}$ , which is clearly higher than what would be expected based  
535 on the  $\text{NO}_2^-$  reduction  $\text{NO}_2^-$  isotope effect of  $<10\%$ . Following the argumentation of Jones et al. (2015), who reported a similar  
536 N isotopic offset between  $\text{NO}_2^-$  and  $\text{N}_2\text{O}$  of  $27.0 \pm 4.5\%$ , this could be indicative for a heavy N accumulating in a forming NO  
537 pool, whereas  $^{14}\text{N}$  is preferentially reacting to  $\text{N}_2\text{O}$  or  $\text{N}_2$ , respectively. This might even be supported by the rather low  $\delta^{15}\text{N}^{\text{bulk}}$   
538 values detected for  $\text{N}_2\text{O}$  in both setups.

539  
540  
541  
542  
543  
544



545 **Table 3: Comparison of the isotope values obtained during dead biomass versus the abiotic experiments. T0 values represent means**  
 546 **calculated by summarizing results across all pH ± standard error.  $\delta^{15}\text{N}$  and  $\delta^{18}\text{O}$  values were calculated using  $\bar{x}_{t_0} - \bar{x}_{t_{end}}$ . Isotope**  
 547 **fractionation was calculated as  $\Delta^{15}\text{N}$  based on the slope between the lowest initial value (here at  $t_1$ ) and  $t_{end}$  for all pH.  $\Delta^{15}\text{N}$  ( $= \delta^{15}\text{N}_{\text{nitrite}} -$**   
 548  **$\delta^{15}\text{N}_{2\text{O}^{\text{bulk}}}$ ) was calculated for the end of the experiment.**

	Dead Biomass	Abiotic
$\delta^{15}\text{N}_{\text{nitrite}(t_0-t_{end})}$	$\downarrow 5.99 \pm 0.65\%$	$\downarrow 5.93 \pm 0.73\%$
$\delta^{18}\text{O}_{\text{nitrite}(t_0-t_{end})}$	$\downarrow 1.75 \pm 0.23\%$	$\downarrow 1.15 \pm 0.18\%$
$^{15}\epsilon_{\text{nitrite}}$	$-10.36\%$ <sup>#</sup>	-
$^{18}\epsilon_{\text{nitrite}}$	$-0.51\%$ <sup>#</sup>	-
<b>SP</b>	$1.17 \pm 1.2\%$	$5.99 \pm 0.84\%$
$\delta^{15}\text{N}^a$	$-51.84 \pm 0.1\%$	$-43.53 \pm 0.16\%$
$\delta^{15}\text{N}^{\text{bulk}}$	$-49.38 \pm 1.01\%$	$-46.48 \pm 2.1\%$
$\Delta^{15}\text{N}$	$23.2\%$	$27.85\%$

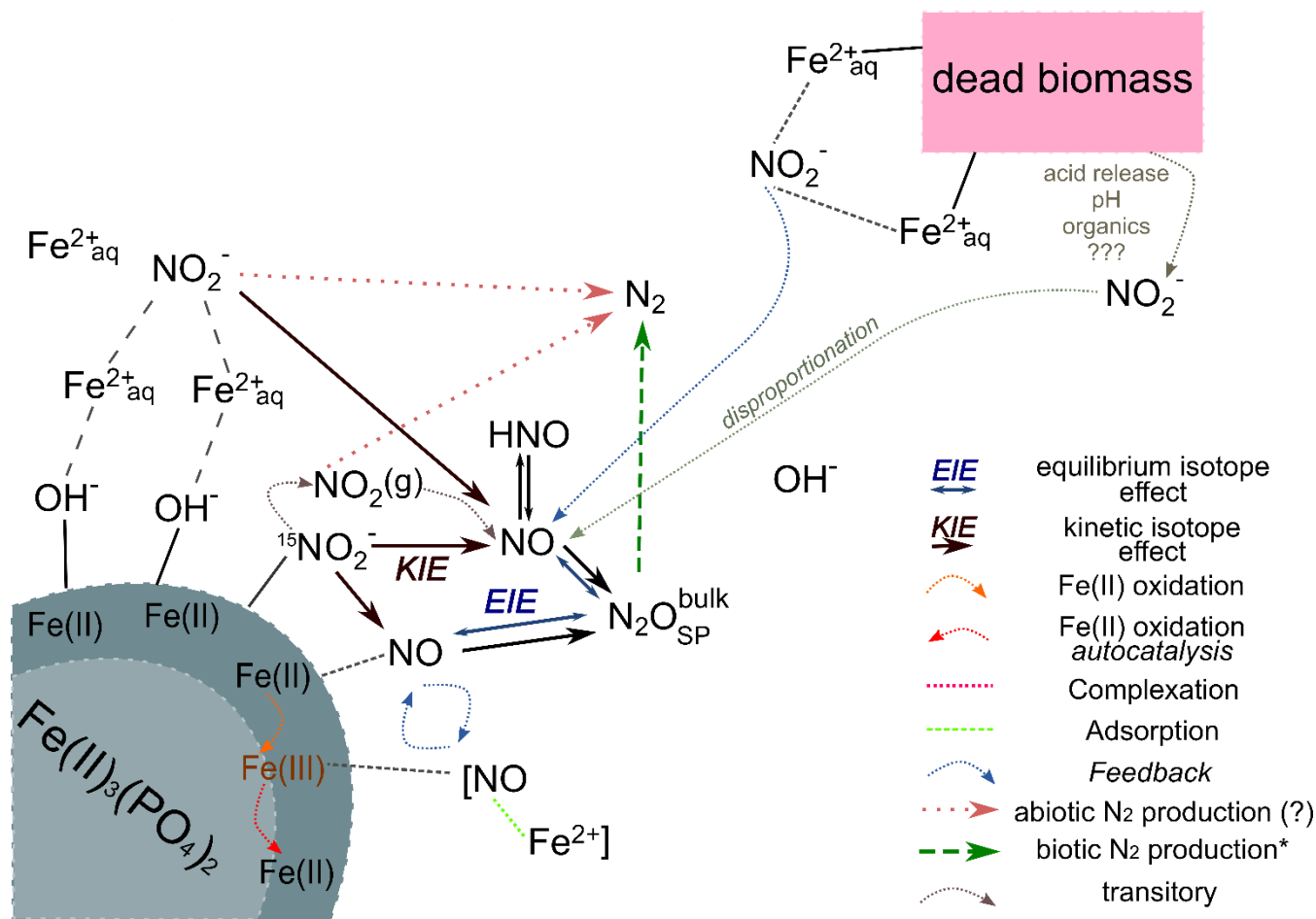
549 <sup>#</sup> n=4 (t1 to tend); - concentrations in abiotic experiment fluctuate and show only minor decrease, hence  $^{15}\epsilon$  and  $^{18}\epsilon$  could not be calculated.  
 550

551 While our results clearly showed that  $\text{N}_2\text{O}$  accumulates over the course of the reaction, it remains unclear, which additional  
 552 end products are present at the final stage of the experiment. If NO accumulates (instead of following the reaction cascade  
 553 further), the substrate-product relationship between the  $\delta^{15}\text{N}\text{-NO}_2^-$  and  $\delta^{15}\text{N}\text{-N}_2\text{O}$  values that would be expected in a closed  
 554 system is perturbed, leading to significantly higher  $\Delta^{15}\text{N}$  than predicted by the  $\delta^{15}\text{N}\text{-NO}_2^-$  trend. Hence, the calculated  $\Delta^{15}\text{N}$  of  
 555 the mineral-only treatment (27.9‰) is only slightly higher than that of the DB experiment (23.2‰), and would therefore  
 556 suggest that despite the differences in chemodenitrification kinetics (i.e., different  $\text{NO}_2^-$  reduction rates and extent), the NO  
 557 pool formed is enriched in heavy N in both treatments, respectively. Alternatively, fractional reduction of the produced  $\text{N}_2\text{O}$   
 558 to  $\text{N}_2$  may also affect the  $\Delta^{15}\text{N}$  since it would presumably increase the  $\delta^{15}\text{N}\text{-N}_2\text{O}$  and thereby raise the low  $\delta^{15}\text{N}\text{-N}_2\text{O}$  closer to  
 559 the starting  $\delta^{15}\text{N}\text{-NO}_2^-$ . Abiotic decomposition of  $\text{N}_2\text{O}$  to  $\text{N}_2$  in the presence of Fe-bearing zeolites has been investigated  
 560 previously (Rivallan et al., 2009), however, it remains unclear if this process could also occur here. Fractional  $\text{N}_2\text{O}$  reduction  
 561 is also not explicitly indicated by the SP values, which would reflect an increase with  $\text{N}_2\text{O}$  reduction (Ostrom et al., 2007;  
 562 Winther et al., 2018). The SP values in both mineral-only and DB-amended experiments were, with some exceptions, relatively  
 563 low ( $6.0 \pm 0.8\%$ ;  $1.7 \pm 1.2\%$ ; Fig. 6). In fact, SP values observed during the course of our experiments are significantly lower  
 564 compared to SP values reported in other studies on Fe-oxide-mineral associated chemodenitrification (e.g., ~16‰; Jones et al.  
 565 (2015); 26.5‰; Grabb et al. 2017), or during the abiotic  $\text{N}_2\text{O}$  production during the reaction of Fe and a  $\text{NH}_2\text{OH}/\text{NO}_2^-$  mixture  
 566 (34‰; Heil et al. 2014). While the variety of different SP values for chemodenitrification-derived  $\text{N}_2\text{O}$  suggests different  
 567 reaction conditions and catalytic effects, our SP data seem to imply that the mineral catalyst plays only a minor role with  
 568 regards to the isotopic composition of the  $\text{N}_2\text{O}$  produced. However, since  $\text{N}_2\text{O}$  concentrations, even if minor, are increasing  
 569 towards the end of the experiments, production and possible decomposition as well as ongoing sorption mechanisms might



570 also serve as possible explanation leading to these rather low SP values. N<sub>2</sub>O SP values have been used as valuable tracer for  
571 microbial N<sub>2</sub>O production (Ostrom & Ostrom, 2012). Based on pure culture studies (Ostrom et al., 2007; Winther et al., 2018;  
572 Wunderlin et al., 2013) and investigations in natural environments (Wenk et al., 2016) a SP range of -10 to 0‰ is considered  
573 to be characteristic for denitrification or nitrifier denitrification (Sutka et al., 2006; Toyoda et al., 2005), whereas higher values  
574 are usually attributed to nitrification or fungal denitrification (Ostrom & Ostrom, 2012; Wankel et al., 2017; Well & Flessa,  
575 2009). The SP values reported here (0 to 10‰) fall well within the range of biological N<sub>2</sub>O production, explicitly denitrification  
576 and soil derived denitrification (2.3 to 16‰) (Ostrom & Ostrom, 2012), rendering the separation between chemodenitrification  
577 and microbial denitrification based on N<sub>2</sub>O isotope measurements difficult, if not impossible.

578 In summary, the N and O isotope systematics of chemodenitrification are multifaceted, depending on the environmental  
579 conditions, reaction partners provided, and/or the speciation of precipitated mineral phases. The systematics observed here are  
580 clearly not entirely governed by normal kinetic isotope fractionation only, as has also been observed in previous work. Grabb  
581 et al. (2017) demonstrated that there is a relationship between reaction rate and kinetic NO<sub>2</sub><sup>-</sup> N and O isotope effects, with  
582 faster reaction leading to lower <sup>15</sup>ε and <sup>18</sup>ε. Again, changes in the expression and even in the direction of the isotope effects in  
583 the NO<sub>2</sub><sup>-</sup> pool suggest that multiple processes, including equilibrium isotope exchange (at least with regards to the δ<sup>18</sup>O- NO<sub>2</sub><sup>-</sup>  
584 ), are contributing to the net N and O isotope fractionation regulated by the experimental conditions and reaction rates. As  
585 pointed out by Grabb et al. (2017), and as supported by our comparative study with pure abiotic mineral phases and with added  
586 dead biomass, the accessibility of Fe(II) to the reaction may be a key factor regarding the degree of N and O isotope  
587 fractionation expressed, particularly if complexation limits the reactive sites of the mineral. The conditions that, at least  
588 transiently, lead to the apparent inverse N and O isotope fractionation observed here for chemodenitrification requires  
589 particular attention by future work. At this point, we can only speculate about potential mechanisms, which are indicated in  
590 the conceptual illustration (Figure 8). As chemodenitrification seems to be catalysed by reactive surfaces of Fe(II)/Fe(III)-  
591 minerals and/or organics (including cells), sorption onto these surfaces might play a crucial role in the fractionation of N and  
592 O isotopes. For example, during the catalytic hydrogenation of CO<sub>2</sub> on Fe and Co catalysts a subtle depletion (ca. 4‰) in  
593 <sup>13</sup>CO<sub>2</sub> at progressed conversion to methane has been explained by the precipitation of a <sup>13</sup>C-enriched carbon intermediate (e.g.,  
594 CO-graphite) on the catalyst surface (Taran et al., 2010). We are fully aware that it is difficult to compare our system with  
595 Fischer-Tropsch synthesis of methane occurring at high temperature and pressure. Yet given the indirect evidence for NO  
596 accumulation in our experiments, it may well be that preferential chemisorption/complexation of “heavy” intermediate NO  
597 occurs, which may lead to transient <sup>15</sup>N-depletion in the reactant NO<sub>2</sub><sup>-</sup> pool. Considering that the N<sub>2</sub>O concentrations measured  
598 in our experiments were comparatively low and that δ<sup>15</sup>N<sup>bulk</sup> N<sub>2</sub>O values did not noticeably change throughout the experiments,  
599 formation of N<sub>2</sub> via abiotic interactions between NO<sub>2</sub><sup>-</sup> and NO may also be involved (Doane, 2017; Phillips et al., 2016). Hence,  
600 N<sub>2</sub>O is meddling with the reaction dynamics either as an intermediate or as a side product, and can thereby influence the overall  
601 N and O isotope dynamics.



602  
 603 **Figure 8: Conceptual figure depicting the proposed reaction mechanisms and feedbacks between the different N species during**  
 604 **chemodenitrification induced by the presence of a mineral surface (lower left corner) or (dead) biomass (upper right corner).**  
 605 **Adsorption of Fe<sup>2+</sup> (directly or via complexation by OH<sup>-</sup>) as well as NO<sub>2</sub><sup>-</sup> could catalyse a direct reaction between both. In addition,**  
 606 **NO<sub>2</sub><sup>-</sup> adsorption onto the Fe(II) mineral might also induce disproportionation, leading to NO<sub>x</sub> formation. These formed**  
 607 **intermediates, although transitory, may impact the overall reaction dynamics by e.g. complex formation (i.e. [NO-Fe<sup>2+</sup>]) or direct**  
 608 **Fe(II) oxidation. The produced Fe(III) might induce another feedback loop (autocatalysis) resulting in further Fe(II) oxidation.**  
 609 **Similar processes are possibly induced by the presence of (dead) biomass. Adsorption and complexation of either NO<sub>2</sub><sup>-</sup> and Fe<sup>2+</sup>**  
 610 **would enhance the reaction between both. In addition, the presence of organic acids would decrease the pH locally and thereby**  
 611 **promote and accelerate NO<sub>2</sub><sup>-</sup> disproportionation and thus additionally enhance Fe(II) oxidation. Our results suggest that NO<sub>2</sub><sup>-</sup>**  
 612 **reduction results in an KIE, which should influence the isotopic composition of NO. N<sub>2</sub>O here is an intermediate, the isotopic**  
 613 **composition of which is mainly influenced by an EIE between NO and N<sub>2</sub>O. The low N<sub>2</sub>O yields as well as the N<sub>2</sub>O isotopic results**  
 614 **(bulk, SP) clearly suggests that N<sub>2</sub> is produced abiotically.**

615





## 616 5. Conclusions and outlook

617 In the absence of any clear (genetic) evidence for enzymatic NDFeO from cultures (e.g. *Acidovorax* sp. strain BoFeN1),  
618 heterotrophic denitrification/ $\text{NO}_3^-$  reduction coupled to abiotic oxidation of Fe(II) with the  $\text{NO}_2^-$  has been presented as the most  
619 reasonable explanation for NDFeO. Here we investigated the second, abiotic step, clearly demonstrating that Fe-associated  
620 abiotic  $\text{NO}_2^-$  reduction can be catalysed by mineral and organic phases under environmentally relevant conditions, as found  
621 for example in soils and aquifers. Our results confirm that reactive surfaces play a major role with regards to the reaction  
622 between  $\text{NO}_2^-$  and Fe(II) and that surface-catalysed chemodenitrification appears to not only contribute to the production of  
623 the greenhouse gas  $\text{N}_2\text{O}$  in environments hosting active cycling of Fe and N, but also to an abiotic production of  $\text{N}_2$ . In order  
624 to understand the mechanistic details of Fe-coupled chemodenitrification, natural-abundance measurements of reactive-N  
625 isotope ratios may help distinguish between abiotic and biotic reactions during NDFeO. Our results, however, indicate that the  
626 potential of coupled N and O isotope measurements to determine the relative importance of Fe-induced N-transformations in  
627 natural environments is somewhat limited. Considering, for example, the apparent inverse N isotope effect in the mineral-only  
628 experiments, our studies show that the  $\text{NO}_2^-$  N vs. O isotope systematics seem to contrast distinctly between biotic and abiotic  
629  $\text{NO}_2^-$  reduction, potentially permitting the disentanglement of the biotic versus abiotic processes.  $\text{N}_2\text{O}$  SP values seem to be  
630 less diagnostic with regards to discriminating between chemodenitrification-derived  $\text{N}_2\text{O}$  and  $\text{N}_2\text{O}$  that is produced during  
631 microbial  $\text{NO}_2^-$  reduction. Our results suggest that both the reaction between Fe(II) and reactive N species, as well as the  
632 resulting isotope effects, are dependent on the reactive surfaces available. The presence of organic material seems to enhance  
633  $\text{NO}_2^-$  reduction and, to a lesser extent also  $\text{N}_2\text{O}$  production, leading to the enrichment in  $^{15}\text{N}$  in the residual  $\text{NO}_2^-$ , as predicted  
634 by Rayleigh-type kinetic N isotope fractionation. In the presence of only Fe(II) minerals,  $\text{NO}_2^-$  reduction rates are significantly  
635 lower, and net N and O isotope effects are not governed by kinetic isotope fractionation only, but also by isotope equilibrium  
636 fractionation during exchange with the ambient mineral phase and/or the ambient water (in the case of O isotopes). While  $\text{N}_2\text{O}$   
637 production was significant, the  $\text{N}_2\text{O}$  yields were below 5%, suggesting that a significant fraction of the  $\text{NO}_2^-$  reduced is at least  
638 transiently transformed to NO and possibly  $\text{N}_2$ . This transient pool of NO possibly stands in quasi-equilibrium with other  
639 intermediates (i.e. HNO,  $\text{NO}_2(\text{g})$ ) or complexes (i.e. Fe-NO), and may thereby impact the overall reaction kinetics as well.  
640 We speculate that the transient accumulation of NO represents an important constraint both on overall reaction kinetics as well  
641 as on the  $\text{N}_2\text{O}$  isotopic signature (or  $\Delta^{15}\text{N}$ ), an aspect that should be verified in future work. Such work may include the  
642 quantification of  $\text{N}_2$  (and its N isotopic composition), which will help to assess to what extent (i) Fe-mineral surface-induced  
643 chemodenitrification leads to the formation of a transient pool of NO and is driven by the catalytically induced abiotic reaction  
644 between Fe(II) and  $\text{NO}_2^-$ , or if (ii) NO is actually the main oxidizing agent of Fe(II).  
645 Our data revealed further complexity with regards to N and O isotope effects during Fe-coupled chemodenitrification than  
646 previously reported. We argue that its isotopic imprint depends on the substrate concentration, the presence of reactive surfaces  
647 or other catalysts, the mechanisms induced by these catalysts (e.g. surface complexation), and putatively on the intermediates  
648 as well as on the product present at the end of the experiments. The multifaceted control on coupled N and O isotope



649 systematics in reactive N species may explain the discrepancies observed between our and previous work (e.g., with regards  
650 to  $^{15}\text{E}:$  $^{18}\text{E}$  ratios; Grabb et al. 2017). Clearly, one has to be realistic with regards to using  $\text{NO}_2^-$  and/or  $\text{N}_2\text{O}$  N and O isotope  
651 measurements to provide constraints on the relative importance of chemodenitrification under natural conditions. Yet, at this  
652 point, there is only a very limited number of studies on the isotope effects of chemodenitrification, and with the results  
653 presented here, we expand the body of work that aims at using stable isotope measurements to assess the occurrence of  
654 chemodenitrification in denitrifying environments. More work on the controls of stable isotope systematics of  
655 chemodenitrification, in particular on the role of reactive, and potentially cryptic, intermediate N species, and of O isotope  
656 exchange, will improve our ability to more quantitatively trace Fe-coupled nitrite reduction and  $\text{N}_2\text{O}$  production in natural Fe-  
657 rich soil or sedimentary environments.

#### 658 **Data availability**

659 Data can be accessed upon request to the corresponding author.

#### 660 **Author contributions**

661 AAK initiated the project. MFL and AAK supervised the project. ANV designed and conducted all experiments. Isotope  
662 measurements as well as data analysis were performed by ANV under the supervision of MFL. JMB conducted Mössbauer  
663 measurements and data analysis. PAN supervised and performed all  $\text{N}_2\text{O}$  concentration determination measurements. ANV,  
664 SDW and MFL interpreted the data and prepared the paper with inputs from all other co-authors.

#### 665 **Competing interests**

666 The authors declare that they have no conflict of interest.

#### 667 **Acknowledgements**

668 Special thanks go to Karen L. Casciotti (Stanford University) for helping with the correction of the  $\text{N}_2\text{O}$  isotope data. Thanks  
669 to Cindy-Louise Lockwood for corrections and comments on earlier versions of the manuscript, and to Viola Warter, Elizabeth  
670 Tomaszewski for fruitful discussions on abiotic chemistry and mineral reactions. Markus Maisch is thanked for his help with  
671 the preparation of the Mössbauer samples.



## 672 **Funding**

673 This research was supported by the Deutsche Forschungsgemeinschaft - DFG (Grants GRK 1708 Molecular principles of  
674 bacterial survival strategies), and through funds from the University of Basel, Switzerland.

## 675 **References**

- 676 Anderson, I. C. and Levine, J. S.: Relative Rates of Nitric Oxide and Nitrous Oxide Production by Nitrifiers, Denitrifiers,  
677 and Nitrate Respirers, *Appl. Environ. Microbiol.*, 51(5), 938–945 [online] Available from:  
678 <http://www.ncbi.nlm.nih.gov/pmc/articles/PMC238991/>, 1986.
- 679 Andrews, S. C., Robinson, A. K., Rodriguez-Quinones, F. and Rodríguez-Quinones, F.: Bacterial iron homeostasis, *Fems*  
680 *Microbiol. Rev.*, 27(2–3), 215–237, doi:10.1016/s0168-6445(03)00055-x, 2003.
- 681 Baumgärtner, M. and Conrad, R.: Role of nitrate and nitrite for production and consumption of nitric oxide during  
682 denitrification in soil, *Fems Microbiol. Lett.*, 101(1), 59–65, doi:10.1111/j.1574-6968.1992.tb05762.x, 1992.
- 683 Braun, V. and Hantke, K.: *The Tricky Ways Bacteria Cope with Iron Limitation*, pp. 31–66, Springer, Dordrecht., 2013.
- 684 Buchwald, C. and Casciotti, K. L.: Isotopic ratios of nitrite as tracers of the sources and age of oceanic nitrite, *Nat. Geosci.*,  
685 6(4), 308–313, doi:10.1038/ngeo1745, 2013.
- 686 Buchwald, C., Grabb, K., Hansel, C. M. and Wankel, S. D.: Constraining the role of iron in environmental nitrogen  
687 transformations: Dual stable isotope systematics of abiotic NO<sub>2</sub>- reduction by Fe(II) and its production of N<sub>2</sub>O, *Geochim.*  
688 *Cosmochim. Acta*, 186, 1–12, doi:<http://dx.doi.org/10.1016/j.gca.2016.04.041>, 2016.
- 689 Casciotti, K. L.: Inverse kinetic isotope fractionation during bacterial nitrite oxidation, *Geochim. Cosmochim. Acta*, 73(7),  
690 2061–2076, doi:10.1016/j.gca.2008.12.022, 2009.
- 691 Casciotti, K. L. and McIlvin, M. R.: Isotopic analyses of nitrate and nitrite from reference mixtures and application to  
692 Eastern Tropical North Pacific waters, *Mar. Chem.*, 107(2), 184–201, doi:10.1016/j.marchem.2007.06.021, 2007.
- 693 Casciotti, K. L., Boehlke, J. K., McIlvin, M. R., Mroczkowski, S. J., Hannon, J. E., Böhlke, J. K., McIlvin, M. R.,  
694 Mroczkowski, S. J. and Hannon, J. E.: Oxygen isotopes in nitrite: Analysis, calibration, and equilibration, *Anal. Chem.*,  
695 79(6), 2427–2436, doi:10.1021/ac061598h, 2007.
- 696 Chakraborty, A., Roden, E. E., Schieber, J. and Picardal, F.: Enhanced growth of *Acidovorax* sp. strain 2AN during nitrate-  
697 dependent Fe(II) oxidation in batch and continuous-flow systems., *Appl. Environ. Microbiol.*, 77(24), 8548–56,  
698 doi:10.1128/AEM.06214-11, 2011.
- 699 Charlet, L., Wersin, P. and Stumm, W.: Surface charge of MnCO<sub>3</sub> and FeCO<sub>3</sub>, *Geochim. Cosmochim. Acta*, 54(8), 2329–  
700 2336, doi:10.1016/0016-7037(90)90059-T, 1990.
- 701 Chen, D., Liu, T., Li, X., Li, F., Luo, X., Wu, Y. and Wang, Y.: Biological and chemical processes of microbially mediated  
702 nitrate-reducing Fe(II) oxidation by *Pseudogulbenkiania* sp. strain 2002, *Chem. Geol.*, 476, 59–69,  
703 doi:10.1016/j.chemgeo.2017.11.004, 2018.



- 704 Choi, P. S., Naal, Z., Moore, C., Casado-Rivera, E., Abruna, H. D., Helmann, J. D. and Shapleigh, J. P.: Assessing the  
705 Impact of Denitrifier-Produced NO on other bacteria, *Appl. Environ. Microbiol.*, 72(3), 2200–2205,  
706 doi:10.1128/aem.72.3.2200-2205.2006, 2006.
- 707 Van Cleemput, O. and Samater, A.: Nitrite in soils: accumulation and role in the formation of gaseous N compounds, *Fertil.*  
708 *Res.*, 45(1), 81–89, doi:10.1007/BF00749884, 1995.
- 709 Coby, A. J. and Picardal, F. W.: Inhibition of NO<sub>3</sub><sup>-</sup> and NO<sub>2</sub><sup>-</sup> reduction by microbial Fe(III) reduction: Evidence of a  
710 reaction between NO<sub>2</sub><sup>-</sup> and cell surface-bound Fe<sup>2+</sup>, *Appl. Environ. Microbiol.*, 71(9), 5267–5274,  
711 doi:10.1128/aem.71.9.5267-5274.2005, 2005.
- 712 Cornell, R. M. and Schwertmann, U.: *The Iron Oxides: Structure, Properties, Reactions, Occurrences and Uses*, 2nd ed.,  
713 Wiley-VCH., 2003.
- 714 Cundy, A. B., Hopkinson, L. and Whitby, R. L. D.: Use of iron-based technologies in contaminated land and groundwater  
715 remediation: A review, *Sci. Total Environ.*, 400(1–3), 42–51, doi:10.1016/j.scitotenv.2008.07.002, 2008.
- 716 Dai, Y.-F., Xiao, Y., Zhang, E.-H., Liu, L.-D., Qiu, L., You, L.-X., Dummi Mahadevan, G., Chen, B.-L. and Zhao, F.:  
717 Effective methods for extracting extracellular polymeric substances from *Shewanella oneidensis* MR-1, *Water Sci. Technol.*,  
718 74(12), 2987–2996, doi:10.2166/wst.2016.473, 2016.
- 719 Delahay, P., Pourbaix, M. and Rysselberghe, P. Van: POTENTIAL-pH DIAGRAMS', *J. Chem. Educ.* [online] Available  
720 from: <https://pubs.acs.org/doi/pdfplus/10.1021/ed027p683> (Accessed 20 April 2018), 1950.
- 721 Dhakal, P.: *Abiotic nitrate and nitrite reactivity with iron oxide minerals*, University of Kentucky., 2013.
- 722 Dhakal, P., Matocha, C. J., Huggins, F. E. and Vandiviere, M. M.: Nitrite Reactivity with Magnetite, *Environ. Sci. Technol.*,  
723 47(12), 6206–6213, doi:10.1021/es304011w, 2013.
- 724 Doane, T. A.: The Abiotic Nitrogen Cycle, *ACS Earth Sp. Chem.*, 1(7), 411–421, doi:10.1021/acsearthspacechem.7b00059,  
725 2017.
- 726 Elsner, M.: Stable isotope fractionation to investigate natural transformation mechanisms of organic contaminants:  
727 principles, prospects and limitations, *J. Environ. Monit.*, 12(11), 2005–2031, doi:10.1039/c0em00277a, 2010.
- 728 Elsner, M., Schwarzenbach, R. P. and Haderlein, S. B.: Reactivity of Fe(II)-Bearing Minerals toward Reductive  
729 Transformation of Organic Contaminants, *Environ. Sci. Technol.*, 38(3), 799–807, doi:10.1021/es0345569, 2004.
- 730 Expert, D.: Iron, an Element Essential to Life, in *Molecular Aspects of Iron Metabolism in Pathogenic and Symbiotic Plant-*  
731 *Microbe Associations*, pp. 1–6, Springer, Dordrecht., 2012.
- 732 Fowle, D. A. and Konhauser, K. O.: *Microbial Surface Reactivity*, pp. 614–616, Springer, Dordrecht., 2011.
- 733 Frame, C. H. and Casciotti, K. L.: Biogeochemical controls and isotopic signatures of nitrous oxide production by a marine  
734 ammonia-oxidizing bacterium, *Biogeosciences*, 7(9), 2695–2709, doi:10.5194/bg-7-2695-2010, 2010.
- 735 Fry, B.: *Stable Isotope Ecology*, 3rd ed., Springer Science+Business Media, LLC, New York., 2006.
- 736 Goretski, J. and Hollocher, T. C.: Trapping of nitric oxide produced during denitrification by extracellular hemoglobin, *J.*  
737 *Biol. Chem.*, 263(5), 2316–2323 [online] Available from: <http://www.jbc.org/content/263/5/2316.abstract>, 1988.



- 738 Gorski, C. A. and Scherer, M. M.: Fe<sup>2+</sup> sorption at the Fe oxide-water interface: A revised conceptual framework, in  
739 Aquatic Redox Chemistry, vol. 1071, edited by P. G. Tratnyek, T. J. Grundl, and S. B. Haderlein, pp. 315–343, ACS  
740 Publications., 2011.
- 741 Grabb, K. C., Buchwald, C., Hansel, C. M. and Wankel, S. D.: A dual nitrite isotopic investigation of chemodenitrification  
742 by mineral-associated Fe(II) and its production of nitrous oxide, *Geochim. Cosmochim. Acta*, 196, 388–402 [online]  
743 Available from: <https://www.sciencedirect.com/science/article/pii/S0016703716306044> (Accessed 28 March 2019), 2017.
- 744 Granger, J. and Sigman, D. M.: Removal of nitrite with sulfamic acid for nitrate N and O isotope analysis with the denitrifier  
745 method, *Rapid Commun. Mass Spectrom.*, 23(23), 3753–3762, doi:10.1002/rcm.4307, 2009.
- 746 Granger, J., Sigman, D. M., Lehmann, M. F. and Tortell, P. D.: Nitrogen and oxygen isotope fractionation during  
747 dissimilatory nitrate reduction by denitrifying bacteria, *Limnol. Oceanogr.*, 53(6), 2533–2545,  
748 doi:10.4319/lo.2008.53.6.2533, 2008.
- 749 Granger, J., Karsh, K. L., Guo, W., Sigman, D. M. and Kritee, K.: The nitrogen and oxygen isotope composition of nitrate in  
750 the environment: The systematics of biological nitrate reduction, *Geochim. Cosmochim. Acta*, 73(13), A460–A460, 2009.
- 751 Halder, S., Yadav, K. K., Sarkar, R., Mukherjee, S., Saha, P., Halder, S., Karmakar, S. and Sen, T.: Alteration of Zeta  
752 potential and membrane permeability in bacteria: a study with cationic agents., *Springerplus*, 4, 672, doi:10.1186/s40064-  
753 015-1476-7, 2015.
- 754 He, H., Zhang, S., Zhu, C. and Liu, Y.: Equilibrium and kinetic Si isotope fractionation factors and their implications for Si  
755 isotope distributions in the Earth's surface environments, *Acta Geochim.*, 35(1), 15–24, doi:10.1007/s11631-015-0079-x,  
756 2016a.
- 757 He, S., Tominski, C., Kappler, A. A., Behrens, S. and Roden, E. E.: Metagenomic analyses of the autotrophic Fe(II)-  
758 oxidizing, nitrate-reducing enrichment culture KS, *Appl. Environ. Microbiol.*, 82(9), 2656–2668, doi:10.1128/AEM.03493-  
759 15, 2016b.
- 760 Heidelberg, J. F., Paulsen, I. T., Nelson, K. E., Gaidos, E. J., Nelson, W. C., Read, T. D., Eisen, J. A., Seshadri, R., Ward, N.,  
761 Methe, B., Clayton, R. A., Meyer, T., Tsapin, A., Scott, J., Beanan, M., Brinkac, L., Daugherty, S., DeBoy, R. T., Dodson,  
762 R. J., Durkin, A. S., Haft, D. H., Kolonay, J. F., Madupu, R., Peterson, J. D., Umayam, L. A., White, O., Wolf, A. M.,  
763 Vamathevan, J., Weidman, J., Impraim, M., Lee, K., Berry, K., Lee, C., Mueller, J., Khouri, H., Gill, J., Utterback, T. R.,  
764 McDonald, L. A., Feldblyum, T. V., Smith, H. O., Venter, J. C., Nealson, K. H. and Fraser, C. M.: Genome sequence of the  
765 dissimilatory metal ion-reducing bacterium *Shewanella oneidensis*, *Nat. Biotechnol.*, 20(11), 1118–1123,  
766 doi:10.1038/nbt749, 2002.
- 767 Heil, J., Vereecken, H. and Brüggemann, N.: A review of chemical reactions of nitrification intermediates and their role in  
768 nitrogen cycling and nitrogen trace gas formation in soil, *Eur. J. Soil Sci.*, 67, 23–39, doi:10.1111/ejss.12306, 2016.
- 769 Hunkeler, D. and Elsner, M.: Principles and Mechanisms of Isotope Fractionation, in *Environmental Isotopes in*  
770 *Biodegradation and Bioremediation*, edited by M. Aelion Höhener, P., Hunkeler, D., pp. 43–76, CRC Press., 2009.
- 771 Ilbert, M. and Bonnefoy, V.: Insight into the evolution of the iron oxidation pathways, *Biochim. Biophys. Acta - Bioenerg.*,



- 772 1827(2), 161–175, doi:<http://dx.doi.org/10.1016/j.bbabi.2012.10.001>, 2013.
- 773 Jamieson, J., Prommer, H., Kaksonen, A. H., Sun, J., Siade, A. J., Yusov, A. and Bostick, B.: Identifying and Quantifying  
774 the Intermediate Processes during Nitrate-Dependent Iron(II) Oxidation, *Environ. Sci. Technol.*, *acs.est.8b01122*,  
775 doi:[10.1021/acs.est.8b01122](https://doi.org/10.1021/acs.est.8b01122), 2018.
- 776 Jones, L. C., Peters, B., Lezama Pacheco, J. S., Casciotti, K. L. and Fendorf, S.: Stable Isotopes and Iron Oxide Mineral  
777 Products as Markers of Chemodenitrification, *Environ. Sci. Technol.*, *49*(6), 3444–3452, doi:[10.1021/es504862x](https://doi.org/10.1021/es504862x), 2015.
- 778 Kampschreur, M. J. M. J., Kleerebezem, R., de Vet, W. W. J. M. J. M. and van Loosdrecht, M. C. M. M.: Reduced iron  
779 induced nitric oxide and nitrous oxide emission, *Water Res.*, *45*(18), 5945–5952,  
780 doi:<http://dx.doi.org/10.1016/j.watres.2011.08.056>, 2011.
- 781 Kendall, C. and Aravena, R.: Nitrate Isotopes in Groundwater Systems, , 261–297, doi:[10.1007/978-1-4615-4557-6\\_9](https://doi.org/10.1007/978-1-4615-4557-6_9), 2000.
- 782 Klueglein, N. and Kappler, A. A.: Abiotic oxidation of Fe(II) by reactive nitrogen species in cultures of the nitrate-reducing  
783 Fe(II) oxidizer *Acidovorax* sp BoFeN1 - questioning the existence of enzymatic Fe(II) oxidation, *Geobiology*, *11*(2), 396,  
784 doi:[10.1111/gbi.12040](https://doi.org/10.1111/gbi.12040), 2013.
- 785 Klueglein, N., Zeitvogel, F., Stierhof, Y.-D., Floetenmeyer, M., Konhauser, K. O., Kappler, A. A. and Obst, M.: Potential  
786 Role of Nitrite for Abiotic Fe(II) Oxidation and Cell Encrustation during Nitrate Reduction by Denitrifying Bacteria, *Appl.*  
787 *Environ. Microbiol.*, *80*(3), 1051–1061, doi:[10.1128/aem.03277-13](https://doi.org/10.1128/aem.03277-13), 2014.
- 788 Kumpiene, J., Lagerkvist, A. and Maurice, C.: Stabilization of As, Cr, Cu, Pb and Zn in soil using amendments – A review,  
789 *Waste Manag.*, *28*(1), 215–225, doi:[10.1016/J.WASMAN.2006.12.012](https://doi.org/10.1016/J.WASMAN.2006.12.012), 2008.
- 790 Lagarec, K. and Rancourt, D. G.: Extended Voigt-based analytic lineshape method for determining N-dimensional correlated  
791 hyperfine parameter distributions in Mössbauer spectroscopy, *Nucl. Instruments Methods Phys. Res. Sect. B Beam Interact.*  
792 *with Mater. Atoms*, *129*(2), 266–280, doi:[10.1016/S0168-583X\(97\)00284-X](https://doi.org/10.1016/S0168-583X(97)00284-X), 1997.
- 793 Laufer, K., Røy, H., Jørgensen, B. B. and Kappler, A. A.: Evidence for the existence of autotrophic nitrate-reducing Fe(II)-  
794 oxidizing bacteria in marine coastal sediment, *Appl. Environ. Microbiol.*, *82*(20), 6120–6131, doi:[10.1128/AEM.01570-16](https://doi.org/10.1128/AEM.01570-16),  
795 2016.
- 796 Li, W., Beard, B. L. and Johnson, C. M.: Exchange and fractionation of Mg isotopes between epsomite and saturated MgSO  
797 4 solution, *Geochim. Cosmochim. Acta*, *75*, 1814–1828, doi:[10.1016/j.gca.2011.01.023](https://doi.org/10.1016/j.gca.2011.01.023), 2011.
- 798 Lies, D. P., Hernandez, M. E., Kappler, A. A., Mielke, R. E., Gralnick, J. A. and Newman, D. K.: *Shewanella oneidensis*  
799 MR-1 uses overlapping pathways for iron reduction at a distance and by direct contact under conditions relevant for  
800 biofilms, *Appl. Environ. Microbiol.*, *71*(8), 4414–4426, doi:[10.1128/aem.71.8.4414-4426.2005](https://doi.org/10.1128/aem.71.8.4414-4426.2005), 2005.
- 801 Liu, J. and Konermann, L.: Irreversible Thermal Denaturation of Cytochrome c Studied by Electrospray Mass Spectrometry,  
802 *J. Am. Soc. Mass Spectrom.*, *20*(5), 819–828, doi:[10.1016/J.JASMS.2008.12.016](https://doi.org/10.1016/J.JASMS.2008.12.016), 2009.
- 803 Liu, J., Wang, Z., Belchik, S. M., Edwards, M. J., Liu, C., Kennedy, D. W., Merkley, E. D., Lipton, M. S., Butt, J. N.,  
804 Richardson, D. J., Zachara, J. M., Fredrickson, J. K., Rosso, K. M. and Shi, L.: Identification and Characterization of MtoA:  
805 A Decaheme c-Type Cytochrome of the Neutrophilic Fe(II)-Oxidizing Bacterium *Sideroxydans lithotrophicus* ES-1., *Front.*



- 806 Microbiol., 3, 37, doi:10.3389/fmicb.2012.00037, 2012.
- 807 Liu, T., Chen, D., Luo, X., Li, X. and Li, F.: Microbially mediated nitrate-reducing Fe(II) oxidation: Quantification of  
808 chemodenitrification and biological reactions, *Geochim. Cosmochim. Acta*, doi:10.1016/J.GCA.2018.06.040, 2018.
- 809 Lovley, D. R.: Microbial Fe(III) reduction in subsurface environments, *FEMS Microbiol. Rev.*, 20(3–4), 305–313,  
810 doi:10.1111/j.1574-6976.1997.tb00316.x, 1997.
- 811 Lovley, D. R.: Electromicrobiology, *Annu. Rev. Microbiol.*, 66(1), 391–409, doi:10.1146/annurev-micro-092611-150104,  
812 2012.
- 813 Luan, F., Liu, Y., Griffin, A. M., Gorski, C. A. and Burgos, W. D.: Iron(III)-Bearing Clay Minerals Enhance Bioreduction of  
814 Nitrobenzene by *Shewanella putrefaciens* CN32, *Env. Sci Technol*, 49, 1418–1476, doi:10.1021/es504149y, 2015.
- 815 Luna-Zaragoza, D., Romero-Guzmán, E. T. and Reyes-Gutiérrez, L. R.: Surface and Physicochemical Characterization of  
816 Phosphates Vivianite,  
817 Fe<sub>2</sub>(PO<sub>4</sub>)<sub>3</sub>  
818 and Hydroxyapatite, Ca<sub>5</sub>(OH)(PO<sub>4</sub>)<sub>3</sub>, *J. Miner. Mater. Charact. Eng.*,  
819 08(08), 591–609, doi:10.4236/jmmce.2009.88052, 2009.
- 820 Mariotti, A., Germon, J. C., Hubert, P., Kaiser, P., Letolle, R., Tardieux, A. and Tardieux, P.: Experimental-Determination of  
821 Nitrogen Kinetic Isotope Fractionation - Some Principles - Illustration for the Denitrification and Nitrification Processes,  
822 *Plant Soil*, 62(3), 413–430, doi:Doi 10.1007/Bf02374138, 1981.
- 823 Martin, T. S. and Casciotti, K. L.: Paired N and O isotopic analysis of nitrate and nitrite in the Arabian Sea oxygen deficient  
824 zone, *Deep. Res. Part I Oceanogr. Res. Pap.*, 121, 121–131, doi:10.1016/j.dsr.2017.01.002, 2017.
- 825 McIlvin, M. R. and Altabet, M. A.: Chemical conversion of nitrate and nitrite to nitrous oxide for nitrogen and oxygen  
826 isotopic analysis in freshwater and seawater, *Anal. Chem.*, 77(17), 5589–5595, doi:10.1021/ac050528s, 2005.
- 827 McIlvin, M. R. and Casciotti, K. L.: Fully automated system for stable isotopic analyses of dissolved nitrous oxide at natural  
828 abundance levels, *Limnol. Oceanogr. Methods*, 8(2), 54–66, doi:10.4319/lom.2010.8.54, 2010.
- 829 McKnight, G. M., Smith, L. M., Drummond, R. S., Duncan, C. W., Golden, M. and Benjamin, N.: Chemical synthesis of  
830 nitric oxide in the stomach from dietary nitrate in humans., *Gut*, 40(2), 211–4 [online] Available from:  
831 <http://www.ncbi.nlm.nih.gov/pubmed/9071933> (Accessed 18 March 2018), 1997.
- 832 Minguzzi, A., Fan, F.-R. F., Vertova, A., Rondinini, S. and Bard, A. J.: Dynamic potential–pH diagrams application to  
833 electrocatalysts for wateroxidation, *Chem. Sci.*, 3(1), 217–229, doi:10.1039/C1SC00516B, 2012.
- 834 Miot, J., Remusat, L., Duprat, E., Gonzalez, A., Pont, S. and Poinso, M. M.: Fe biomineralization mirrors individual  
835 metabolic activity in a nitrate-dependent Fe(II)-oxidizer, *Front. Microbiol.*, 6(SEP), 879, doi:10.3389/fmicb.2015.00879,  
836 2015.
- 837 Mohn, J., Wolf, B., Toyoda, S., Lin, C.-T., Liang, M.-C., Brüggemann, N., Wissel, H., Steiker, A. E., Dyckmans, J., Szvec,  
838 L., Ostrom, N. E., Casciotti, K. L., Forbes, M., Giesemann, A., Well, R., Doucett, R. R., Yarnes, C. T., Ridley, A. R., Kaiser,  
839 J. and Yoshida, N.: Interlaboratory assessment of nitrous oxide isotopomer analysis by isotope ratio mass spectrometry and



- 840 laser spectroscopy: current status and perspectives, *Rapid Commun. Mass Spectrom.*, 28(18), 1995–2007,  
841 doi:10.1002/rcm.6982, 2014.
- 842 Muehe, E. M., Gerhardt, S., Schink, B. and Kappler, A.: Ecophysiology and the energetic benefit of mixotrophic Fe(II)  
843 oxidation by various strains of nitrate-reducing bacteria, *FEMS Microbiol. Ecol.*, 70(3), 335–343, doi:10.1111/j.1574-  
844 6941.2009.00755.x, 2009.
- 845 Muehe, E. M., Obst, M., Hitchcock, A., Tyliczszak, T., Behrens, S., Schröder, C., Byrne, J. M., Michel, F. M., Krämer, U.  
846 and Kappler, A. A.: Fate of Cd during microbial Fe(III) mineral reduction by a novel and Cd-tolerant geobacter species,  
847 *Environ. Sci. Technol.*, 47(24), 14099–14109, doi:10.1021/es403365w, 2013.
- 848 Nelson, D. W. and Bremner, J. M.: Factors affecting chemical transformations of nitrite in soils, *Soil Biol. Biochem.*, 1(3),  
849 229–239, doi:10.1016/0038-0717(69)90023-6, 1969.
- 850 Niklaus, P. A., Le Roux, X., Poly, F., Buchmann, N., Scherer-Lorenzen, M., Weigelt, A. and Barnard, R. L.: Plant species  
851 diversity affects soil–atmosphere fluxes of methane and nitrous oxide, *Oecologia*, 181(3), 919–930, doi:10.1007/s00442-  
852 016-3611-8, 2016.
- 853 Nordhoff, M., Tominski, C., Halama, M., Byrne, J. M., Obst, M., Kleindienst, S., Behrens, S. and Kappler, A. A.: Insights  
854 into nitrate-reducing Fe(II) oxidation mechanisms through analysis of cell-mineral associations, cell encrustation, and  
855 mineralogy in the chemolithoautotrophic enrichment culture KS, *Appl. Environ. Microbiol.*, 83(13), e00752-17,  
856 doi:10.1128/AEM.00752-17, 2017.
- 857 Ostrom, N. E. and Ostrom, P.: *Handbook of Environmental Isotope Geochemistry*, 1st ed., edited by M. Baskaran, Springer  
858 Berlin Heidelberg, Berlin, Heidelberg., 2011.
- 859 Ostrom, N. E. and Ostrom, P. H.: The Isotopomers of Nitrous Oxide: Analytical Considerations and Application to  
860 Resolution of Microbial Production Pathways, in *Handbook of Environmental Isotope Geochemistry: Vol I*, edited by M.  
861 Baskaran, pp. 453–476, Springer Berlin Heidelberg, Berlin, Heidelberg., 2012.
- 862 Ostrom, N. E., Pitt, A., Sutka, R., Ostrom, P. H., Grandy, A. S., Huizinga, K. M. and Robertson, G. P.: Isotopologue effects  
863 during N<sub>2</sub>O reduction in soils and in pure cultures of denitrifiers, *J. Geophys. Res.*, 112(G2), doi:10.1029/2006jg000287,  
864 2007.
- 865 Ostrom, N. E., Gandhi, H., Coplen, T. B., Toyoda, S., Böhlke, J. K., Brand, W. A., Casciotti, K. L., Dyckmans, J.,  
866 Giesemann, A., Mohn, J., Well, R., Yu, L. and Yoshida, N.: Preliminary assessment of stable nitrogen and oxygen isotopic  
867 composition of USGS51 and USGS52 nitrous oxide reference gases and perspectives on calibration needs, *Rapid Commun.*  
868 *Mass Spectrom.*, 32(15), 1207–1214, doi:10.1002/rcm.8157, 2018.
- 869 Otte, J. M., Blackwell, N., Ruser, R., Kappler, A. A., Kleindienst, S. and Schmidt, C.: N<sub>2</sub>O formation by nitrite-induced  
870 (chemo)denitrification in coastal marine sediment, *Sci. Rep.*, 9(1), 10691, doi:10.1038/s41598-019-47172-x, 2019.
- 871 Ottley, C. J., Davison, W. and Edmunds, W. M.: Chemical catalysis of nitrate reduction by iron(II), *Geochim. Cosmochim.*  
872 *Acta*, 61(9), 1819–1828, doi:Doi 10.1016/S0016-7037(97)00058-6, 1997.
- 873 Pereira, C., Ferreira, N. R., Rocha, B. S., Barbosa, R. M. and Laranjinha, J.: The redox interplay between nitrite and nitric





- 874 oxide: From the gut to the brain, *Redox Biol.*, 1(1), 276–284, doi:<http://dx.doi.org/10.1016/j.redox.2013.04.004>, 2013.
- 875 Phillips, R. L., Song, B., McMillan, A. M. S., Grelet, G., Weir, B. S., Palmada, T. and Tobias, C.: Chemical formation of  
876 hybrid di-nitrogen calls fungal codenitrification into question, *Sci. Rep.*, 6(1), 39077, doi:[10.1038/srep39077](https://doi.org/10.1038/srep39077), 2016.
- 877 Piasecki, W., Szymanek, K. and Charmas, R.: Fe 2+ adsorption on iron oxide: the importance of the redox potential of the  
878 adsorption system, *Adsorption*, doi:[10.1007/s10450-019-00054-0](https://doi.org/10.1007/s10450-019-00054-0), 2019.
- 879 Piepenbrock, A., Dippon, U., Porsch, K., Appel, E. and Kappler, A. A.: Dependence of microbial magnetite formation on  
880 humic substance and ferrihydrite concentrations, *Geochim. Cosmochim. Acta*, 75(22), 6844–6858,  
881 doi:[10.1016/j.gca.2011.09.007](https://doi.org/10.1016/j.gca.2011.09.007), 2011.
- 882 Price, A., Macey, M. C., Miot, J. and Olsson-Francis, K.: Draft Genome Sequences of the Nitrate-Dependent Iron-Oxidizing  
883 Proteobacteria *Acidovorax* sp. Strain BoFeN1 and *Paracoccus pantotrophus* Strain KS1, edited by J. C. Thrash, *Microbiol.*  
884 *Resour. Announc.*, 7(10), e01050-18, doi:[10.1128/mra.01050-18](https://doi.org/10.1128/mra.01050-18), 2018.
- 885 Rakshit, S., Matocha, C. J. and Coyne, M. S.: Nitrite reduction by siderite, *Soil Sci. Soc. Am. J.*, 72(4), 1070–1077,  
886 doi:[10.2136/sssaj2007.0296](https://doi.org/10.2136/sssaj2007.0296), 2008.
- 887 Rancourt, D. G. and Ping, J. Y.: Voigt-based methods for arbitrary-shape static hyperfine parameter distributions in  
888 Mössbauer spectroscopy, *Nucl. Instruments Methods Phys. Res. Sect. B Beam Interact. with Mater. Atoms*, 58(1), 85–97,  
889 doi:[10.1016/0168-583X\(91\)95681-3](https://doi.org/10.1016/0168-583X(91)95681-3), 1991.
- 890 Rivallan, M., Ricchiardi, G., Bordiga, S. and Zecchina, A.: Adsorption and reactivity of nitrogen oxides (NO<sub>2</sub>, NO, N<sub>2</sub>O) on  
891 Fe-zeolites, *J. Catal.*, 264(2), 104–116, doi:[10.1016/j.jcat.2009.03.012](https://doi.org/10.1016/j.jcat.2009.03.012), 2009.
- 892 Samarkin, V. A., Madigan, M. T., Bowles, M. W., Casciotti, K. L., Priscu, J. C., McKay, C. P. and Joye, S. B.: Abiotic  
893 nitrous oxide emission from the hypersaline Don Juan Pond in Antarctica, *Nat. Geosci.*, 3(5), 341–344,  
894 doi:[10.1038/ngeo847](https://doi.org/10.1038/ngeo847), 2010.
- 895 Schaefer, M. V.: Spectroscopic evidence for interfacial Fe(II)- Fe(III) electron transfer in clay minerals, Iowa Research  
896 Online. [online] Available from: <http://ir.uiowa.edu/etd/596> (Accessed 20 March 2018), 2010.
- 897 Sigman, D. M., DiFiore, P. J., Hain, M. P., Deutsch, C., Wang, Y., Karl, D. M., Knapp, A. N., Lehmann, M. F. and Pantoja,  
898 S.: The dual isotopes of deep nitrate as a constraint on the cycle and budget of oceanic fixed nitrogen, *Deep. Res. Part I-*  
899 *Oceanographic Res. Pap.*, 56(9), 1419–1439, doi:[10.1016/j.dsr.2009.04.007](https://doi.org/10.1016/j.dsr.2009.04.007), 2009.
- 900 Snyder, L. R. and Adler, H. J.: Dispersion in Segmented Flow through Glass Tubing in Continuous-Flow Analysis: The Ideal  
901 Model, *Anal. Chem.*, 48(7), 1017–1022, doi:[10.1021/ac60371a013](https://doi.org/10.1021/ac60371a013), 1976.
- 902 Sorensen, J. and Thorling, L.: Stimulation by Lepidocrocite (Gamma-Fe<sub>2</sub>O<sub>3</sub>) of Fe(II)-Dependent Nitrite Reduction,  
903 *Geochim. Cosmochim. Acta*, 55(5), 1289–1294, doi:[Doi 10.1016/0016-7037\(91\)90307-Q](https://doi.org/10.1016/0016-7037(91)90307-Q), 1991.
- 904 Stevenson, F. J., Harrison, R. M., Wetselaar, R. and Leeper, R. A.: Nitrosation of Soil Organic Matter: III. Nature of Gases  
905 Produced by Reaction of Nitrite with Lignins, Humic Substances, and Phenolic Constituents Under Neutral and Slightly  
906 Acidic Conditions<sup>1</sup>, *Soil Sci. Soc. Am. J.*, 34(3), 430, doi:[10.2136/sssaj1970.03615995003400030024x](https://doi.org/10.2136/sssaj1970.03615995003400030024x), 1970.
- 907 Stookey, L. L.: FERROZINE - A NEW SPECTROPHOTOMETRIC REAGENT FOR IRON, *Anal. Chem.*, 42(7), 779-



- 908 doi:10.1021/ac60289a016, 1970.
- 909 Straub, K. L., Benz, M., Schink, B. and Widdel, F.: Anaerobic, nitrate-dependent microbial oxidation of ferrous iron, *Appl.*  
910 *Environ. Microbiol.*, 62(4), 1458–1460, 1996.
- 911 Stumm, W. and Sulzberger, B.: The cycling of iron in natural environments: Considerations based on laboratory studies of  
912 heterogeneous redox processes, *Geochim. Cosmochim. Acta*, 56(8), 3233–3257, doi:10.1016/0016-7037(92)90301-X, 1992.
- 913 Sutka, R. L., Ostrom, N. E., Ostrom, P. H., Breznak, J. A., Gandhi, H., Pitt, A. J. and Li, F.: Distinguishing nitrous oxide  
914 production from nitrification and denitrification on the basis of isotopomer abundances, *Appl. Environ. Microbiol.*, 72(1),  
915 638–644, doi:10.1128/Aem.72.1.638-644.2006, 2006.
- 916 Tanford, C.: Protein denaturation: Part c. theoretical models for the mechanism of denaturation, *Adv. Protein Chem.*, 24(C),  
917 1–95, doi:10.1016/S0065-3233(08)60241-7, 1970.
- 918 Taran, Y. A., Klinger, G. A., Cienfuegos, E. and Shuykin, A. N.: Carbon and hydrogen isotopic compositions of products of  
919 open-system catalytic hydrogenation of CO<sub>2</sub>: Implications for abiogenic hydrocarbons in Earth’s crust, *Geochim.*  
920 *Cosmochim. Acta*, 74(21), 6112–6125, doi:10.1016/j.gca.2010.08.012, 2010.
- 921 Tian, T., Zhou, K., Xuan, L., Zhang, J.-X., Li, Y.-S., Liu, D.-F. and Yu, H.-Q.: Exclusive microbially driven autotrophic  
922 iron-dependent denitrification in a reactor inoculated with activated sludge, *Water Res.*, 170, 115300,  
923 doi:10.1016/j.watres.2019.115300, 2020.
- 924 Tiso, M. and Schechter, A. N.: Nitrate reduction to nitrite, nitric oxide and ammonia by gut bacteria under physiological  
925 conditions., *PLoS One*, 10(3), e0119712, doi:10.1371/journal.pone.0119712, 2015.
- 926 Tominski, C., Heyer, H., Lösekann-Behrens, T., Behrens, S. and Kappler, A. A.: Growth and Population Dynamics of the  
927 Anaerobic Fe(II)-Oxidizing and Nitrate-Reducing Enrichment Culture KS, edited by F. E. Löffler, *Appl. Environ.*  
928 *Microbiol.*, 84(9), e02173-17, doi:10.1128/AEM.02173-17, 2018.
- 929 Toyoda, S. and Yoshida, N.: Determination of Nitrogen Isotopomers of Nitrous Oxide on a Modified Isotope Ratio Mass  
930 Spectrometer, , doi:10.1021/AC9904563, 1999.
- 931 Toyoda, S., Mutobe, H., Yamagishi, H., Yoshida, N. and Tanji, Y.: Fractionation of N<sub>2</sub>O isotopomers during production by  
932 denitrifier, *Soil Biol. Biochem.*, 37(8), 1535–1545, doi:10.1016/j.soilbio.2005.01.009, 2005.
- 933 Veeramani, H., Alessi, D. S., Suvorova, E. I., Lezama-Pacheco, J. S., Stubbs, J. E., Sharp, J. O., Dippon, U., Kappler, A. A.,  
934 Bargar, J. R. and Bernier-Latmani, R.: Products of abiotic U(VI) reduction by biogenic magnetite and vivianite, *Geochim.*  
935 *Cosmochim. Acta*, 75(9), 2512–2528, doi:10.1016/j.gca.2011.02.024, 2011.
- 936 Wankel, S. D., Ziebis, W., Buchwald, C., Charoenpong, C., De Beer, Di., Dentinger, J., Xu, Z. and Zengler, K.: Evidence for  
937 fungal and chemodenitrification based N<sub>2</sub>O flux from nitrogen impacted coastal sediments, *Nat. Commun.*, 8(1), 15595,  
938 doi:10.1038/ncomms15595, 2017.
- 939 Weber, K. A., Hedrick, D. B., Peacock, A. D., Thrash, J. C., White, D. C., Achenbach, L. A. and Coates, J. D.: Physiological  
940 and taxonomic description of the novel autotrophic, metal oxidizing bacterium, *Pseudogulbenkiania* sp strain 2002, *Appl.*  
941 *Microbiol. Biotechnol.*, 83(3), 555–565, doi:10.1007/s00253-009-1934-7, 2009.



- 942 Well, R. and Flessa, H.: Isotopologue signatures of N<sub>2</sub>O produced by denitrification in soils, *J. Geophys. Res.*, 114,  
943 doi:10.1029/2008jg000804, 2009.
- 944 Wenk, C. B., Frame, C. H., Koba, K., Casciotti, K. L., Veronesi, M., Niemann, H., Schubert, C. J., Yoshida, N., Toyoda, S.,  
945 Makabe, A., Zopfi, J. and Lehmann, M. F.: Differential N<sub>2</sub>O dynamics in two oxygen-deficient lake basins revealed by  
946 stable isotope and isotopomer distributions, *Limnol. Oceanogr.*, 61(5), 1735–1749, doi:10.1002/lno.10329, 2016.
- 947 White, G. F., Edwards, M. J., Gomez-Perez, L., Richardson, D. J., Butt, J. N. and Clarke, T. A.: Mechanisms of Bacterial  
948 Extracellular Electron Exchange, in *Advances in Microbial Physiology*, vol. 68, pp. 87–138., 2016.
- 949 Widdel, F. and Pfennig, N.: STUDIES ON DISSIMILATORY SULFATE-REDUCING BACTERIA THAT DECOMPOSE  
950 FATTY-ACIDS .1. ISOLATION OF NEW SULFATE-REDUCING BACTERIA ENRICHED WITH ACETATE FROM  
951 SALINE ENVIRONMENTS - DESCRIPTION OF DESULFOBACTER-POSTGATEI GEN-NOV, SP-NOV, *Arch.*  
952 *Microbiol.*, 129(5), 395–400, doi:10.1007/bf00406470, 1981.
- 953 Widdel, F., Kohring, G.-W. and Mayer, F.: Studies on Dissimilatory Sulfate-Reducing Bacteria that Decompose Fatty Acids,  
954 *Arch Microbiol*, 134, 286–294 [online] Available from: <https://link.springer.com/content/pdf/10.1007/BF00407804.pdf>  
955 (Accessed 22 April 2018), 1983.
- 956 Wilson, W. W., Wade, M. M., Holman, S. C. and Champlin, F. R.: Status of methods for assessing bacterial cell surface  
957 charge properties based on zeta potential measurements, *J. Microbiol. Methods*, 43(3), 153–164, doi:10.1016/S0167-  
958 7012(00)00224-4, 2001.
- 959 Winther, M., Balslev-Harder, D., Christensen, S., Priemé, A., Elberling, B., Crosson, E. and Blunier, T.: Continuous  
960 measurements of nitrous oxide isotopomers during incubation experiments, *Biogeosciences*, 15(3), 767–780,  
961 doi:10.5194/bg-15-767-2018, 2018.
- 962 Wunderlin, P., Lehmann, M. F., Siegrist, H., Tuzson, B., Joss, A., Emmenegger, L. and Mohn, J.: Isotope Signatures of N<sub>2</sub>  
963 O in a Mixed Microbial Population System: Constraints on N<sub>2</sub> O Producing Pathways in Wastewater Treatment, *Environ.*  
964 *Sci. Technol.*, 130118101927005, doi:10.1021/es303174x, 2013.
- 965 Ye, R. W., Averill, B. A. and Tiedje, J. M.: Denitrification: production and consumption of nitric oxide, *Appl. Environ.*  
966 *Microbiol.*, 60(4), 1053–1058 [online] Available from: <http://www.ncbi.nlm.nih.gov/pmc/articles/PMC201439/>, 1994.
- 967 Zeitvogel, F., Burkhardt, C. J., Schroepel, B., Schmid, G., Ingino, P. and Obst, M.: Comparison of Preparation Methods of  
968 Bacterial Cell-Mineral Aggregates for SEM Imaging and Analysis Using the Model System of *Acidovorax sp.* BoFeN1,  
969 *Geomicrobiol. J.*, 34(4), 317–327, doi:10.1080/01490451.2016.1189467, 2017.
- 970 Zumft, W. G.: Cell biology and molecular basis of denitrification, *Microbiol. Mol. Biol. Rev.*, 61(4), 533–+ [online]  
971 Available from: <http://www.ncbi.nlm.nih.gov/pubmed/9409151> (Accessed 19 February 2018), 1997.
- 972 Zweier, J. L., Samouilov, A. and Kuppasamy, P.: Non-enzymatic nitric oxide synthesis in biological systems, *Biochim.*  
973 *Biophys. Acta - Bioenerg.*, 1411(2–3), 250–262, doi:10.1016/S0005-2728(99)00018-3, 1999.
- 974